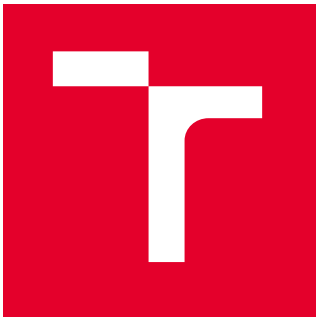

BRNO UNIVERSITY OF TECHNOLOGY

VYSOKÉ UČENÍ TECHNICKÉ V BRNĚ

FACULTY OF ELECTRICAL ENGINEERING AND COMMUNICATION

FAKULTA ELEKTROTECHNIKY
A KOMUNIKAČNÍCH TECHNOLOGIÍ

DEPARTMENT OF RADIO ELECTRONICS

ÚSTAV RADIOELEKTRONIKY

SENSORS FOR ELECTROMAGNETIC DETECTION OF PARTIAL DISCHARGES

SNÍMAČE PRO ELEKTROMAGNETICKOU DETEKCI ČÁSTEČNÝCH VÝBOJŮ

BACHELOR'S THESIS
BAKALÁŘSKÁ PRÁCE

AUTHOR — **Natália Pločeková**
AUTOR PRÁCE

SUPERVISOR — **doc. Ing. Petr Drexler, Ph.D.**
VEDOUCÍ PRÁCE

BRNO 2023

BRNO UNIVERSITY OF TECHNOLOGY
FACULTY OF ELECTRICAL ENGINEERING AND COMMUNICATION

Bachelor's Thesis

Bachelor's study program **Electronics and Communication Technologies**

Department of Radio Electronics

Student: Natália Pločeková ***ID:*** 230302

Year of study: 3 ***Academic year:*** 2022/23

TITLE OF THESIS:

Sensors for electromagnetic detection of partial discharges

INSTRUCTION:

Process a research of a diagnostic and localization of partial discharges using the detection of their electromagnetic radiation in ultra-high frequency band. Study the possibilities of design and implementation of sensors for the detection of transient electrical phenomena through radiated electromagnetic field. Discuss the possibilities of using external sensors to detect partial discharges in power transformers. Propose a possible design of an external sensor of transient electromagnetic phenomena with regard to its possible use for the detection of partial discharges in power transformers.

Built an experimental prototype of the external sensor of partial discharges. Set up an experiment to verify the properties of the designed external sensor. Carry out experimental measurements and compare the obtained results with theoretical assumptions. Based on the obtained conclusions, propose a possible modification for real use of the external sensor in the detection and localization of partial discharges.

RECOMMENDED LITERATURE:

[1] DREXLER, Petr, et al. A Sensor System for Detecting and Localizing Partial Discharges in Power Transformers with Improved Immunity to Interferences. Sensors. 2019, 19(4).

[2] ZHANG, X., ZHANG, G., LI, Y., ZHANG, J., HUANG, R. On the Feasibility of Gap Detection of Power Transformer Partial Discharge UHF Signals: Gap Propagation Characteristics of Electromagnetic Waves. Energies. 2017, 10(10).

Date of project specification: 6.2.2023 ***Deadline for submission:*** 29.5.2023

Supervisor: doc. Ing. Petr Drexler, Ph.D.

doc. Ing. Lucie Hudcová, Ph.D.
Chair of study program board

ABSTRACT

This bachelor thesis is focused on the design of an external type of UHF sensor, which will be placed in the gap of the transformer vessel. First, the waveguide-to-coax adapter is simulated in Ansys HFSS software. Based on the piece of knowledge, the sensor was constructed. The sensor uses two types of waveguide couplers for measuring, monopole probe and loop coupling. The simulated and constructed sensor is then compared for functionality and sensitivity.

KEYWORDS

Power transformers, partial discharges, UHF method, external sensors, current probes and loop probes, waveguide-to-coax adapter, Ansys HFSS software

ABSTRAKT

Tato bakalářská práce se zabývá návrhem externího typu UHF sensoru, který bude umístněný na štěrbině transformátorové nádoby. V prvním kroku byl vlnovod-koax adaptér simulován v programu Ansys HFSS. Na základě poznatků byl zkonstruován sensor. Sensor využívá pro měření dva typy buzení vlnovodu, buzení proudovou sondou a buzení magnetickou smyčkou. Simulovaný a vyrobený sensor je porovnán z hlediska funčnosti a citlivosti.

KLÍČOVÁ SLOVA

Výkonové transformátory, částečné výboje, UHF metoda, externí senzory, buzení proudovou sondou a buzení magnetickou smyčkou, vlnovod-koax adaptér, Ansys HFSS software

ROZŠÍŘENÝ ABSTRAKT

Výroba, distribuce a trh elektrické energie jsou důležité prvky pro fungovaní stát, a proto je nesmírně důležitá spolehlivost. Jedním z důležitějších prvků jsou výkonové transformátory, které zajištují transformaci pro vedení velmi vysokého napětí (VVN) 220kV, a zvláště vysokého napětí (ZVN) 400kV. Tým se zabezpečuje účinnější dálkový přenos energie. Jednou z vysoce namáhaných vnitřních částí výkonových transformátorů je jejích izolace, nejčastěji zajištována strukturou olej-papír. Protože se v této izolaci vyskytují určité nedokonalosti jako například vzduchové bubliny a zároveň je zde přítomné elektrického pole velké intenzity, dochází k výskytu tzv. částečných výbojů (ČV). Při častějším a dlouhodobějších výskytů částečných výbojů dochází postupně k snižovaní kvality oleje a tým aj jeho izolační schopnosti. Proto je nesmírně důležité se snažit o monitorovaní přítomnosti částečných výbojů.

Vznik částečných výbojů je doprovázený emisí světla, zvuku, tepla, elektromagnetické energie či určitými chemickými reakcemi. Metody zachytávaní přítomnosti částečného výbojů jsou různé a vzájemně se mezi sebou odlišují právě tým, kterým fyzikálním či chemickým projevem částečného výboje se zaobírají. Akustické metody jsou založeny na měření zvykových projevů, chemická metoda zkoumá změnu chemického složení izolace a optická metoda se zaobírá emisi světla. Nejvíc používaná metoda je galvanická. Táto metoda je též nazývaná IEC 60270, protože její specifikace jsou dány normou se stejným značením. Pro měření přítomnosti částečných výbojů se používají také elektromagnetické sondy. Při vzniku částečného výboje dochází k vyzáření energie ve formě elektromagnetické vlny. Tento projev využívají jak kapacitní sondy, tak induktivní sensory HFCT ale také i UHF sensory.

Sensor navrhovaný v této práci využívá právě ke své funkci UHF metodu. Hlavní výhodou této metody je její citlivost, elektromagnetická odolnost vůči okolitými rušení a možnost za určitých podmínek lokalizaci částečného výboje. Základní součástí UHF sensoru je anténa, která zabezpečuje proměnu energie elektromagnetické vlny na elektrický signál, který je následně zpracován. UHF sensory využívají různé velikosti a typy antén, které pracují s rozdílnými frekvencemi. Primárně se sensory rozlišují na vnitřní a vnější. Vnitřní se zavádí už při konstrukci a používají se málokdy. Vnější sensory bud využívají dielektrické okno nebo se připojují ku štěrbinám na transformátorové nádobě. Obe varianty mají své výhody a nevýhody. Táto bakalářská práce je zaměřená na návrh vnějšího typu sensoru, který by bol schopný na základě přiložení ke štěrbině analyzovat přítomnost částečných výbojů. Tým by nemuselo byt měření závislé na přítomnosti dielektrických oken. Za určitých podmínek je možné také analyzovat místo vzniku částečného výboje. K tomu se využívá metoda TDOA (Time Differencies of Arrival). Táto metoda potřebuje vícero sensoru umístněných na různých místech. V budoucnosti je možné návrh sensoru

rozšířit i o snahu lokalizovat místo vzniku částečného výboje. V tomto případě však šlo pouze o ověření funkcionality metody.

Transformátorová nádoba je složená z dvou kusů: vrchního a spodního. Tyto kusy jsou spojeny pomocí kovových šroubů. Mezi těmito dvěma kusy se nachází gumové těsnění, které brání uniku oleje z nádoby. Těsnění se nachází jenom v části štěrbiny, kromě toho je tvořena vzduchem. Předpokládaná výška štěrbiny je 6 milimetru. Elektromagnetická vlna se šíří od zdroje signálu prostorem transformátorové nádoby. Následně narazí na štěrbinu, kterou se dále šíří i skrz těsnění. Na konci štěrbiny dochází k difrakci signálu. Snímaní navrhovaného sensoru je tedy založeno na detekci pronikajícího vlnění. Štěrbina je tvořena dvěma rovnoběžnými kovovými stěnami. Na úseku se opakují šrouby, které drží vrchní a spodní část pokope. Jednotlivý úsek vytváří strukturu vlnovodu obdélníkového průřezu. Rozteč šroubu určuje mezní kmitočet vlnovodu. Ze zaslaných materiálů byla určená hodnota rozteče šroubu na hodnotu 130 milimetrů. Pomoci vzorců vysvětlených v práci byla dopočítaný mezní kmitočet. Jeho hodnota je 1,15GHz. To znamená, že z transformátorové nádoby budou schopny uniknout pouze signály s kmitočtem vyšším jako je mezní kmitočet. Existují 3 základní typy buzení vlnovodů: buzení proudovou sondou, magnetickou smyčkou nebo vazebním otvorem. Sensor využívá pouze prvé dva. Také počítá s tým, že jak je možné buzení vlnovodu, tj. přeměna elektrického signálu na elektromagnetické pole, je možná i opačná cesta. Tedy proměna energie elektrického pole na elektrický signál, který by se šířil koaxiálním kabelem a byl by dále analyzovaný. Na tomto principu jsou založeny koax-vlnovod a vlnovod-koax adaptéry. Při buzení proudovou sondou je část koaxiálního kabelu vložena do vnitřka vlnovodu. Sonda se umisťuje v místě maximální intenzity elektrického pole, kde se nachází $\lambda_g/4$ od konce vlnovodu. S pomocí výpočtů uvedených v práci je třeba umístit sondu 53 milimetrů od zadní steny sensoru. Při buzení magnetickou smyčkou je koaxiální kabel vyformován do uzavřené smyčky a vložen kolmo k magnetickým siločarám vidu TE_{10}. Střed smyčky se nachází v místě maximální intenzity magnetického pole. Jako materiál navrhovaného sensoru s vlastnostmi podobnými vlnovodu, byl zvolen FR-4 substrát jednostranně plátovaný mědí. Povrch měděného plátování byl chemicky postříbřen pro zlepšení vodivost.

Při návrhu byli využívaný simulace v programu ANSYS HFSS. Cílem bylo ověření teoretických předpokladů o chování adapteru v elektromagnetickém poli a šíření signálu aperturou. Zároveň byla potvrzena poloha maxim elektrického a magnetického pole. V simulacích bylo zjištěno, že nejmenší utlum signálu při přechodě mezi štěrbinu a sensorem nastává při co nejmenší rozdílu výšek připojeného sensoru a štěrbiny. Je ale na druhé straně třeba počítat s určitou výškou, která je potřeba na pevně upevnění sensoru a jeho fyzickou stabilitu. Bylo zvoleno, že sensor bude mít výšku 20 milimetrů.

Na základě teoretických poznatků a zjištění ze simulaci byla provedena výroba. Jak už bylo zmíněno, sensor je vyroben z FR-4 substrát jednostranně pokrytého stříbrem. Jednotlivé desky byli k sebe připájeny. V stěnách sensoru byli vyřezaný otvory pro vložení sond. Bylo rozhodnuto, že senzorový box bude osazen oběma typy sond – proudovou i indukční (magnetickou smyčkou). Navíc pro porovnaní citlivosti a chování různých velikostí byla každá sonda vyrobena ve dvou rozměrech.

Měření zhotoveného sensoru byli prováděna v stíněné komoře. Během měření se používali 2 antény, jedna vysílací a druha přijímací, která snímala velikost intenzity přítomného elektrického pole. Měření bylo zpracováváno pomocí vektorového analyzátoru. Výsledkem měření bolo určení hodnot S_{21} parametru a anténního faktoru pro různé kmitočty. V měření byl potvrzen předpoklad, že sonda s většími rozměry je citlivější a dochází k menšímu útlumu. Zároveň byl zkoumán vliv naklonění a natočení sensoru. Měření ukázali, že na citlivost sensoru má mnohem vetší vliv natočení sensoru v horizontálním směru jako naklonění ve vertikálním směru. Na konci práce se nachází porovnaní hodnot anténního faktoru simulovaného a vyrobeného adaptéru. Jejich hodnoty se odlišují jenom částečně, co vede k závěrů, že návrh a následně výroba sensoru může být považována jako úspěšní.

PLOČEKOVÁ, Natália. *Sensors for electromagnetic detection of partial discharges*. Brno: Brno University of Technology, Fakulta elektrotechniky a komunikačních technologií, Department of Radio Electronics, 2023, 69 p. Bachelor's Thesis. Advised by doc. Ing. Petr Drexler, Ph.D.

Author's Declaration

Author:	Natália Pločeková
Author's ID:	230302
Paper type:	Bachelor's Thesis
Academic year:	2022/23
Topic:	Sensors for electromagnetic detection of partial discharges

I declare that I have written this paper independently, under the guidance of the advisor and using exclusively the technical references and other sources of information cited in the paper and listed in the comprehensive bibliography at the end of the paper.

As the author, I furthermore declare that, with respect to the creation of this paper, I have not infringed any copyright or violated anyone's personal and/or ownership rights. In this context, I am fully aware of the consequences of breaking Regulation § 11 of the Copyright Act No. 121/2000 Coll. of the Czech Republic, as amended, and of any breach of rights related to intellectual property or introduced within amendments to relevant Acts such as the Intellectual Property Act or the Criminal Code, Act No. 40/2009 Coll. of the Czech Republic, Section 2, Head VI, Part 4.

Brno ....

author's signature*

*The author signs only in the printed version.

ACKNOWLEDGEMENT

I would like to thank the advisor of my thesis, doc. Ing. Petr Drexler, Ph.D. for helpful consultations, patience and his valuable comments. I appreciate the opportunity to work on such an interesting topic and with such an experienced mentor. I also would like to extend my gratitude to Ing. Tomáš Kříž, Ph.D. for his time and useful words of advice on the Ansys software programme.

Contents

List of Figures

Introduction

Power engineering is a segment of electrical engineering focused on the generation, transmission and distribution of energy. The electrical power network of providers and customers is called the electrical grid and is connected by transmission and distribution lines. The electrical grid with transmission and distribution lines should provide uninterrupted power supply from generating plants to consumers and should be reliable and stable. One of the potential threats is a power transformer failure or especially a power transformer insulation failure. To reduce this risk of failure, a systematic study of transformation failures with real data collection is required.

In the power transformer, there is high voltage field stress and therefore there occur partial discharges. The mechanism of these discharges will be explained in Chapter 1. Partial discharges are accompanied by the emission of sound, light, heat, electromagnetic energy or chemical reactions. The measurement methods are various and are distinguished from each other by the procedure they use to identify the partial discharge. The most common methods are explained in Chapter 2.

Chapter 3 is dedicated to the UHF method, especially to UHF sensors and the external type of UHF sensors. This type was used for the design of our sensor. The sensor will be placed on the outer wall of the transformer tank - in the gap. This gap behaves as a waveguide; therefore, the beginning of Chapter 4 belongs to waveguides. In this section, there is also calculated the cut-off frequency of the designed waveguide. In Chapter 4, there are also waveguide couplers and waveguide-to-coax adapters. They include numerous propositions of dimensions of the waveguide with functional components such as monopole antenna and loop.

It was necessary to perform the aperture simulation in the Ansys HFSS software. The simulations in Chapter 5 help determine the behaviour of the electric and magnetic fields for different frequencies and dimensions of the adapter.

The construction of the adapter is explained in Chapter 6. In the beginning of the chapter, the simplification of the real model is mentioned in order to make the manufacture of the sensor easier. The constructed sensor is then tested in the full radio-frequency anechoic chamber. The specifications of the measured parameters and results are found in Chapter 7. The end of the chapter is dedicated to comparing the sensitivity of the simulated and constructed sensor.

1 Partial discharges

1.1 Power transformers

An important part of the electrical grid is the electrical substation, which often includes power transformers. At the beginning of the electrical grid, there are power stations: nuclear power plants, hydroelectric power stations, wind power farms and thermal power plants. They use nuclear, fossil, or renewable sources and convert them into energy. After the generation, there is the electric power transmission; in the electrical substation, transformers step up the voltage. The increase in voltage causes a decrease in current, which means smaller energy losses as the current flows through the conducting wire and the resistance transforms energy to heat loss. This effect is also known as Joule heating. Produced energy is transmitted over long distances by high voltage power lines. In the Czech Republic, these high voltage power lines have 400kV and 220kV. The last stage of the electrical grid is the distribution grid, which distributes electricity to the customers. As it arrives at the point of consumption, another electrical substation steps down the voltage. Firstly, the voltage is lowered to 110kV voltage and then to 22kV - 35kV voltage.

In the Czech Republic, there are two nuclear power plants - Dukovany and Temelín. Dukovany is the first nuclear power plant built in the Czech Republic and now there are four production units. It produces around 15 TWh of electricity annually, covering approximately 20 % of the total consumption of electricity[1]. Temelín has two production units and produces more than 15 TWh per year [2]. Every power plant has several power block transformers. Block transformers provide a transformation of the voltage level of production blocks to a higher level used for long-distance transmission. The transformer is a static machine that consists of a magnetic circuit - core, electrical circuit, terminals, bushings, tank and some other parts. The core of the transformer carries magnetic flux, and the transformer has low-voltage and high-voltage coils. The laminated core is supposed to support the windings of the transformer, which may then carry current in the transformer and produce working magnetic flux. The transformer has two kinds of winding: primary and secondary winding based on the input or output of the supply or high and low voltage winding based on the voltage level of the supply. The tank provides a shelter for the core and windings and is also a container for oil used as a coolant. Terminals and bushings connect the incoming and outgoing supply and load cables. The most important parts of the transformer are shown in Figure 1.1.

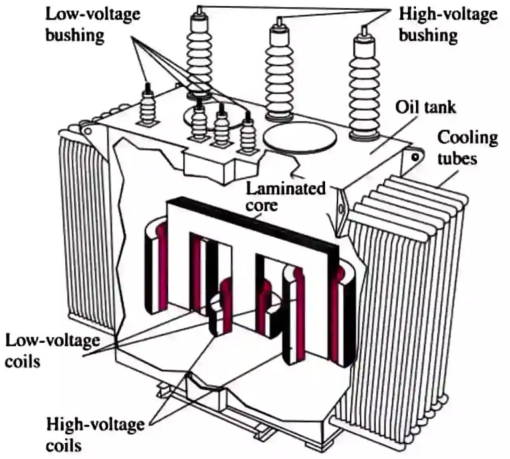

Fig. 1.1: The most important parts of transformer [4]

1.2 Introduction to a partial discharge

Inside the transformation tank, there is an intense electrical field and insulation degradation is considered as one of the main reasons for power transformer failures. Underestimating the bad insulation condition can lead to devastating damage to power transformers, for example, electrical arc or fire. Insulating materials are highly dielectric and heat resistant in order to to protect the transformer from short circuits, discharges, and overheating. Distribution transformers have two types of insulation: solid and transformer oil. Solid insulation is located between the windings and is made of cellulose base such as pressboard and paper [3]. The solid insulation of the power transformer used in the Temelin nuclear plant is shown in Figure 1.2.

Fig. 1.2: Solid insulation of power transformer 2AT3 in ETE used in Temelin

Solid insulation is used as electrical insulation and is the weakest part of the transformer insulation system, easily damaged by generated short circuits or partial discharges [3]. Transformer oil provides electrical insulation and cools the winding and core. It is refined hydro-carbon mineral oil and is composed of aromatics, paraffin, naphthenes, and olefins [4]. Due to solid insulation failures, partial discharges occur in transformer oil and cause deterioration of the transformer oil condition. It causes insufficient oil circulation and consequently overheating of the transformer. Moisture and oxygen together with heat cause oil contamination, which increases the probability of other partial discharges.

Defined by IEC 60270, "partial discharge is a localised electrical discharge that only partially bridges the insulation between conductors and which may or may not occur adjacent to a conductor" [14]. International Standard IEC 60270 defines the terms that are used for the measurements of partial discharges, specifies the quantities that should be measured and defines measuring methods.

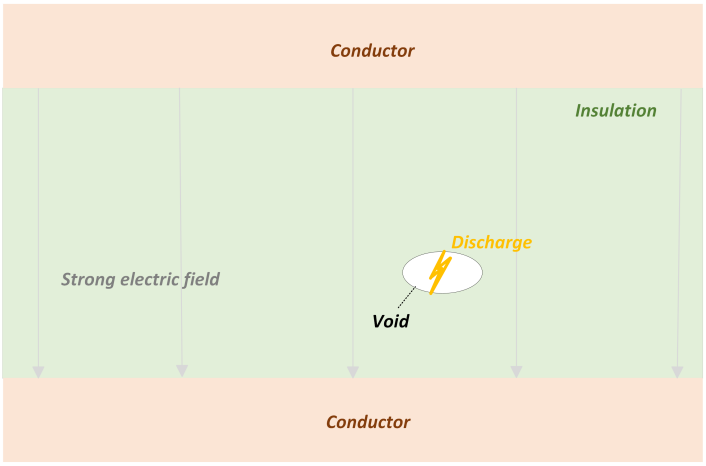

Fig. 1.3: Explanation of a partial discharge mechanism

In Figure 1.3, the partial discharge mechanism is shown. There are two conductors and solid insulation between them. As a result of solid transformation failure, there is a gas filled void and an intense electrical field. This combination can cause a high-frequency transient current pulse in the void, which is termed partial discharge.

Even though the duration of partial discharges is tens of nanoseconds, they can cause a transformer failure, and we need to pay attention to precise diagnostic PD measurements.

2 Detection of partial discharge

2.1 Acoustic detection

The acoustic method analyses pressure waves produced from the vaporisation of the material in the oil around partial discharge due to rapid increase in temperature. A partial discharge monitoring system is mainly composed of a sensor, pre-amplifier, filter, and data acquisition and processing unit [6]. The block diagram of this system is shown in Figure 2.1. A preamplifier amplifies the signal. The filter then eliminates interfering signals, and the rest is amplified in an adjustable amplifier. This signal goes to the oscilloscope or to the threshold block with the preset level to decide if the given pulse represents a partial discharge event. The number of pulses over the defined value is countered in the counter module, which is reset after a defined interval. Eventually, the pulse rate is sent to the PD rate activity visualizer.

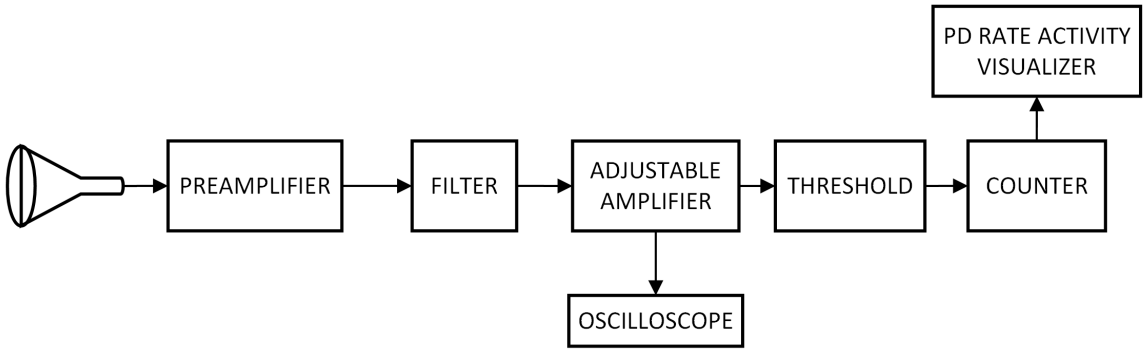

Fig. 2.1: Simplified block diagram of the acoustic detection system

Acoustic sensors are made of piezoelectric crystals and these sensors can be installed externally on the wall of the transformation tank [7]. The sensors can be divided into two categories according to bandwidth and sensitivity. Narrowband sensors are more sensitive but are recommended for a small frequency range: 20-100 kHz. Broadband sensors have a wide frequency range: up to 1MHz.
The advantages of this method are definitely simplicity, the price of the monitoring system, electromagnetic susceptibility, the possibility of spatial localisation of PD and also the option of online monitoring. On the other hand, due to the absorption and refraction of the acoustic signal, one of the biggest disadvantages of this method is the lower sensitivity.

In the second place, there is a combination of acoustic and optical method analyzing changes in optical parameters such as wavelength, intensity, polarization,

and phase. There are four types of optical sensors based on changes in parameters: spectrum-based sensor, intensity-based sensor, polarization-based sensor and interferometric-based sensor [7]. The fiber optic acoustic sensor are made of intrinsic optical fiber sensors such as Michelson and Mach-Zehnder interferometers or Fabry-Perot interferometric sensors [7]. The second sensor mentioned includes a light source launched into a 2×2 coupler. The 3 dB coupler is connected to the sensor head via a single-mode fiber. The other output of the coupler is connected to a photodetector. The optical signal is converted into an electrical signal, amplified, and then processed by a digital oscilloscope or high-speed signal processor. This method has many pros, for example, a small size of sensors, high sensitivity, large bandwidth and electromagnetic susceptibility.

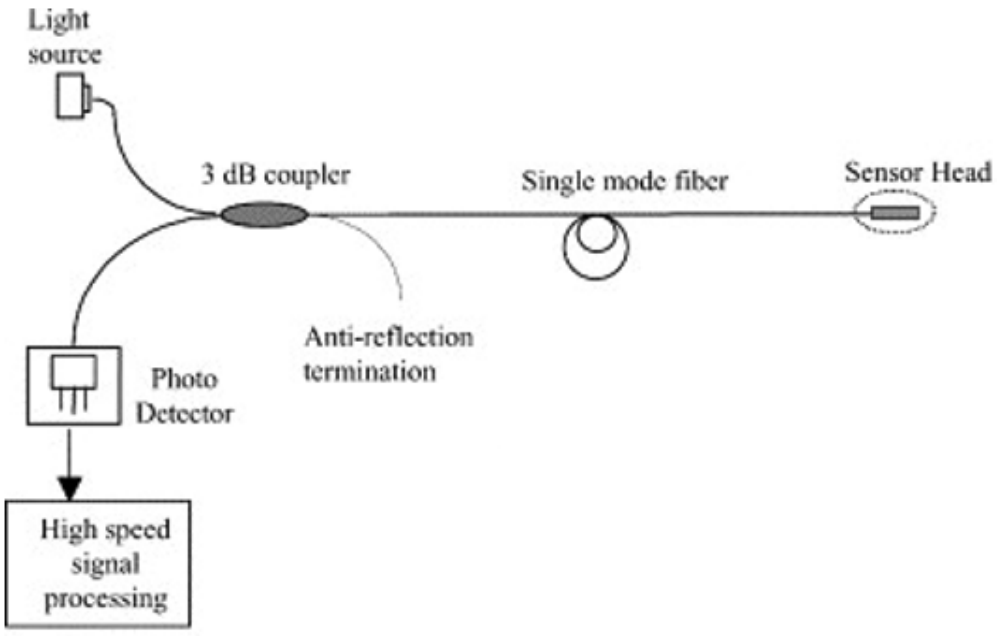

Fig. 2.2: Illustration of the principle of fiber optic acoustic sensor [7]

A comparison of the acoustic method signals with the physical acoustic sensor and the optical method signals with the fiber sensor is shown in Figure 2.3. The output signals from these different sensors have some common traits: both display impulse-like waveforms with a gradually decreasing amplitude and both sensors detect the same time period of about 8 μs. It means that both identified the partial discharge impulse at the typical frequency of the partial discharge acoustic wave (120kHz) [8]. On the other side, when the acoustic wave passes through the insulation, its amplitude rapidly decreases.

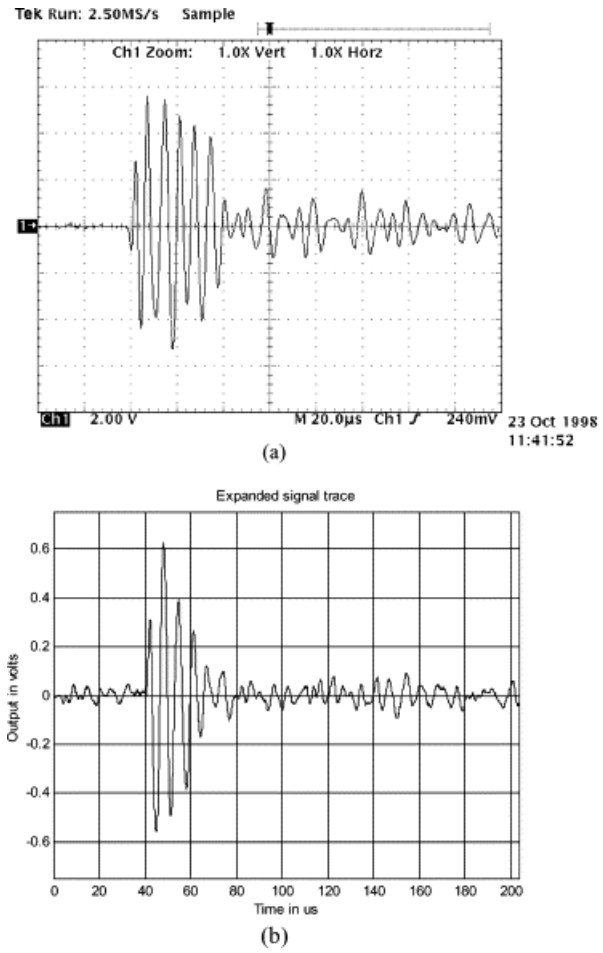

Fig. 2.3: Typical partial discharge acoustic signals detected by (a) physical acoustic sensor and (b) fiber optic sensor. Both sensors are located at a certain distance away from the partial discharge source [8]

2.2 Chemical detection

Chemical technique is based on high performance liquid chromatography (HPLC) or dissolve gas analysis (DGA). The second mentioned test the oil of the transformer tank for the exceeding level of gases such as methane, acetylene, carbon dioxide, ethylene, and hydrogen [7]. The high liquid chromatography (HPLC) test analyses the by-products of the transformer insulation breakdown - mainly glucose. Chemical detection has lower accuracy because there is no standard correlation between the amount of glucose released during insulation breakdown and the type and degree of high-voltage transformer fault [7]. Furthermore, this method cannot determine the exact position of the partial discharge. The DGA test uses a hydrogen-oil detector. The semi-permeable membrane is installed in the transformer tank and then connected to a portable gas chromatograph, which measures the concentration of hydrogen gas every few hours [7].

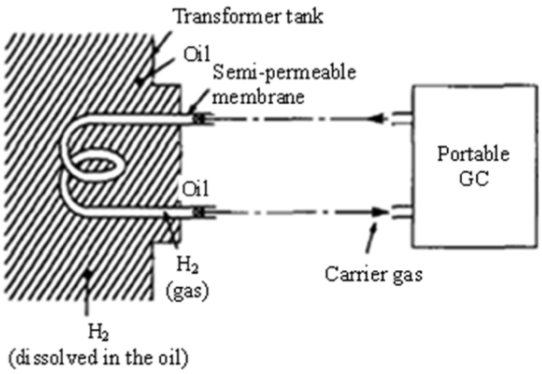

Fig. 2.4: Hydrogen-oil detector for DGA method of PD detection [7]

2.3 Electrical detection

2.3.1 IEC 60270

The electrical method of partial discharge detection is strictly defined by the international standard for the measurement of electrical discharges in insulation - IEC 60270. This method is applicable for alternating voltages up to 400 Hz and direct voltage. The measuring system involves the coupling and measuring unit. The measurement system consists of a high voltage source, a high voltage filter, a coupling capacitor, measuring impedance and PD detector [14]. The apparatus is shown in Figure 2.5. HV filter blocks the noise and interference from the power supply. The filter, called the blocking impedance, blocks the signal from the test object, which increases the sensitivity. The coupling capacitor has a low impedance and passes the high frequency discharge current from PD source. The measuring impedance transforms the input current signal into an output voltage signal. The PD detector detects the partial discharge signal. Additional descriptions of the system, such as the correct selection and configuration, are specified in the standard IEC 60270.

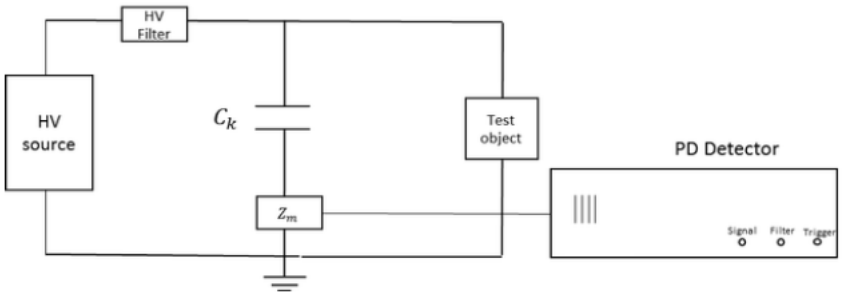

Fig. 2.5: Schematic of the PD measurement setup [14]

2.3.2 HFCT

Another type of electrical sensor, which is related to the measurement of emitted current, is the high frequency current transformer (HFCT) sensor. HFCT sensors are widely used to detect partial discharge not only in power transformers but also in power cables, cable accessories and switchgear [13]. This method is widely used mainly because of the possibility of an online monitoring system and good electrical isolation of the measurement facility. HFCT sensors convert transient current into corresponding inducted voltage measured over the input impedance of the measuring and monitoring equipment (usually 50 Ω) [12].

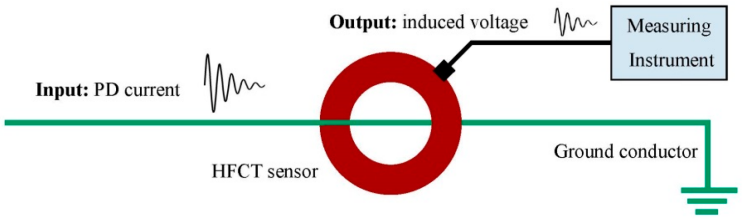

Fig. 2.6: HFCT sensor clamped in a ground conductor for PD measurement [12]

Usually, the HFCT sensor has a bandwidth of 100kHz to 20MHz and it is designed to measure much lower current than the power frequency current carried by a high voltage circuit. This method is accurate at high frequencies, but is unreliable at low frequencies. Partial discharge usually creates short transient current pulses with a few nanosecond rise time. A spectrum of this signal has some significant high-frequency components that are, consequently, filtered. The HFCT sensor catches only signals with a frequency below 10 MHz and uses them for the detection and localization of partial discharge [12]. In Figure 2.7, there is the clamp-type HFCT sensor and the frequency response. The HFCT sensor is composed of an induction coil with a ferromagnetic core and is installed around the grounding conductor of the earthing network.

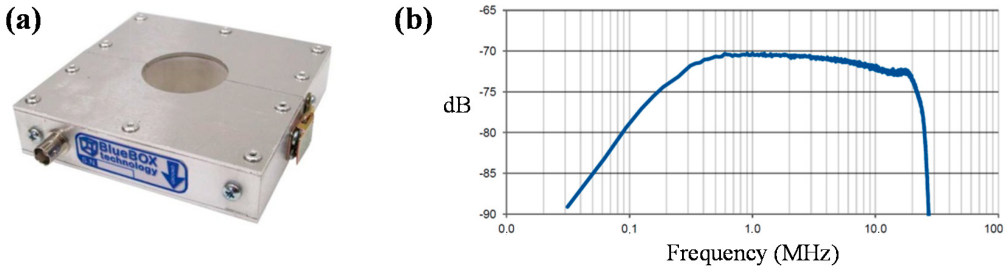

Fig. 2.7: Clamp type HFCT sensor (a) and Frequency response (b) [12]

2.4 Electromagnetic detection

2.4.1 TEV

Transient Earth Voltage Method (TEV) detects manifestation of the electromagnetic waves generated from a partial discharge. The setup of the TEV detection method is shown in Figure 2.8. The TEV sensors are attached to the outer wall of the transformer tank. Emitted electromagnetic waves leak from the insulation in the metal transformer tank. This energy is transformed into surface current flowing on the outside surface of the transformer's vessel. TEV sensors can detect current due to the skin effect, which means that the current flows mainly at the surface of a conductor, in our case the metal tank of the transformer. Meanwhile, another discharge current flows to the ground through the bushings and ground line. The measurement apparatus is made of three components: a non-intrusive sensor, a high-pass filter, and data storage or display equipment [10]. The non-intrusive sensor is located on the external surface of the metallic transformer tank and measures the surface current. The sensor has a metal cover to shield the interference from surroundings. The high-pass filter generates a sharp impulsive waveform with a short decrease in time and cleans the signal from low-frequency disturbances [10]. An oscilloscope or a digitizer with computer is used for data acquisition, processing and visualization. The advantages of this method are high-sensitivity and non-intrusive sensors.

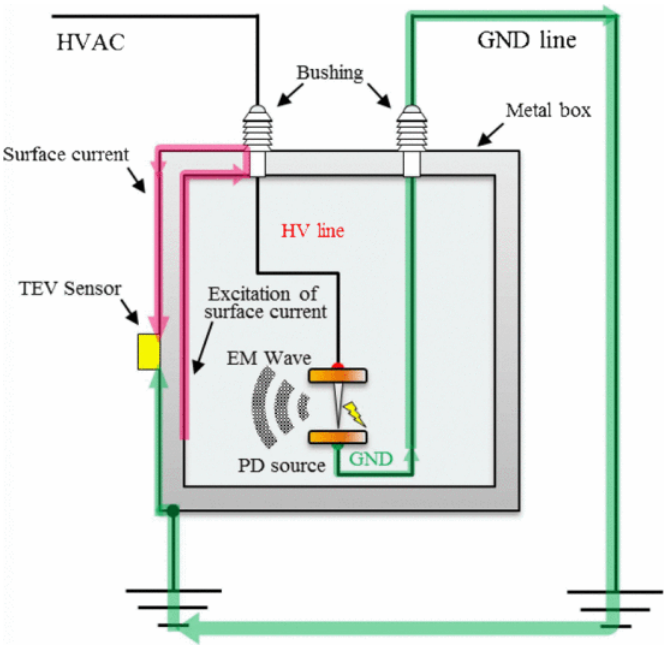

Fig. 2.8: Principle of TEV detection of signals for a metal tank with bushings [9]

2.4.2 UHF detection method

The ultra high frequency method is one of the most popular methods for detecting partial discharges in transformers. The principle and diagrams are shown in Figure 2.9 . In the presence of an intensive electric field, a partial discharge causes the transfer of electrons in a tiny current impulse of very small duration in micro void gaps. This impulse lasts a few nanoseconds. It induces an ultra high frequency signal with frequency range between 300 MHz and 3 GHz (UHF band), plotted in Figure 2.9c. The velocity of emitted electromagnetic waves depends on the permittivity of the transformer oil. There are certain advantages, such as wide detection range, potentially high sensitivity, good electromagnetic immunity against disturbance due to presence of metal transformer tank and possibility of real-time detection and evaluation.

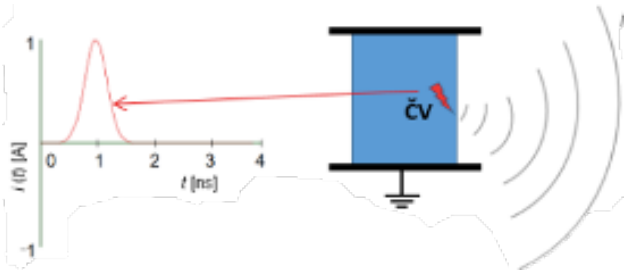

(a) Production of electromagnetic wave from an incurred tiny current impulse i.e. partial discharge

(b) Intensity of electric field component of EM wave radiated by partial discharge

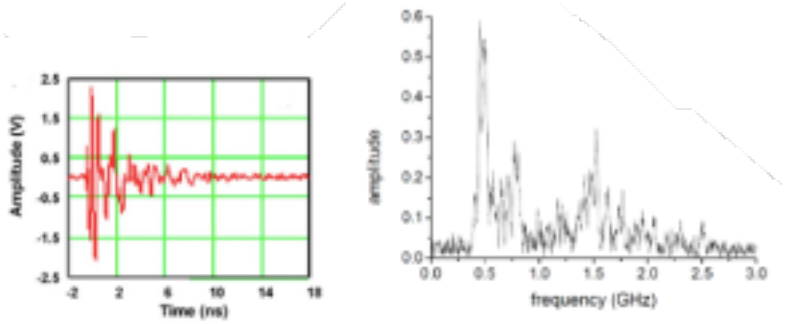

(c) Voltage versus time (left) and frequency spectrum (right) diagram of partial discharge

Fig. 2.9: Explanation of emission of UHF signal and its current, voltage and frequency diagrams

UHF sensors can be mounted inside and outside of the transformer tank and therefore there are two types: internal and external. Internal UHFs are placed inside the transformer tank during construction, and they are rare. External UHF

are more common, and they are fitted in inspection windows or exposed barrier edges. Both types have some issues. The built-in UHF sensors can potentially affect the electrical field and increase a risk of electrical discharge. The external type usually uses a dielectric window and cannot be used in the power transformers in service [16]. The basic setup for the UHF method is shown in Figure 2.10. UHF sensor detects the signal, which is then filtered and amplified. Eventually, the signal is digitized and stored in order to provide additional information. These pieces of information are used for identifying the particular position of partial discharge source.

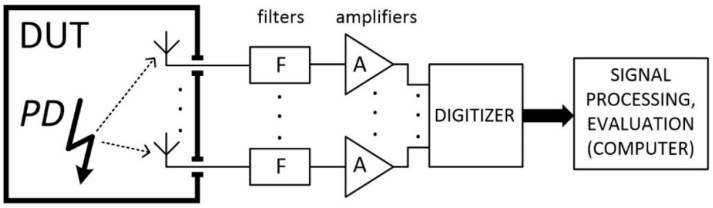

Fig. 2.10: The basic setup for UHF method [15]

The most common method used for partial discharge localisation is the time difference of arrival (TDOA). It needs multiple sensors attached to the outer wall of the transformer tank. A generated signal will reach different sensors placed at different positions at different time according to distance from the partial discharge source. The signal processing system, usually a computer, determines the first peak or other typical feature of the signal related to its time representation and the time difference between the first peaks or features of different signals from multiple sensors. The electromagnetic waves generated from partial discharge are scattered in many directions. They strike a transformer parts, e.g. a tank, coils or solid insulation, some of the energy may be absorbed and the other are bounce off. Therefore, there are even more waves and the detected signal is a superposition of all directed and reflected EM waves with strong time dispersion, as illustrated in 2.11.

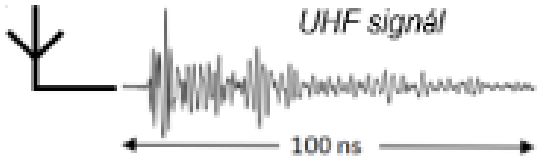

Fig. 2.11: Antenna measurement of complex response of partial discharge in time domain composed of directed and reflected waves inside transformer tank

3 PD UHF external sensor

3.1 UHF sensors

The main part of the UHF sensor is an antenna. It provides the transformation of the energy of an electromagnetic wave into an electrical signal that can be recorded and further processed. There are various types of antennas with different sizes, working frequencies and radiation patterns. Several types of antennas often used for partial discharge detection are shown in Figure 3.1 and are introduced below [18]:

- Monopole antennas are widely used due to their simple structure. These antennas have a narrow working bandwidth, which can cause information loss. In addition, they are less efficient in small sizes. In the case of simplified monopole antennas application, their second pole is substituted by a conductive plane represented by a metal wall of the transformer tank.
- A special type of monopole antenna is a conical antenna, which has better gain and good performance in 300 MHz - 1 GHz.
- Micro-strip antennas have a small thickness, low fabrication cost and small volume. These antennas also have a narrow working bandwidth with high ohmic and dielectric loss.
- Trapezoidal monopole has characteristics similar to the straight-wire monopole antenna but shows a better gain.
- Helix antenna has considerably less gain than other types.
- Vivaldi antenna is a simple broadband planar antenna with linear polarization. An Antipodal Vivaldi antenna is also recommended for the design of UHF sensors.

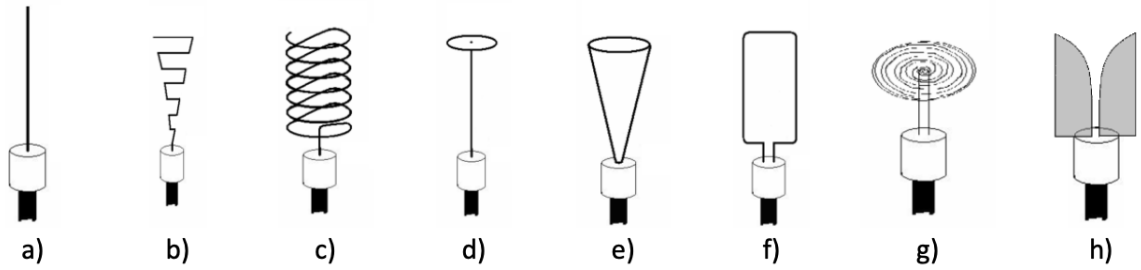

Fig. 3.1: Different types of antennas used in UHF sensors: a) Straight wire Monopole, b) Trapezoidal Monopole, c). Helix Monopole, d) Disc Monopole, e) Conical Monopole, f) Small Loop Antenna, g) Spiral Antenna, h) Vivaldi Antenna [17]

3.2 External UHF sensors

Even though classic external sensors fitted in dielectric windows are more common in transformers, there are certain drawbacks already mentioned above. Due to the mentioned bottlenecks of the built-in sensor and the dielectric window method, there is a willingness to improve the application of the other type of external UHF PD detector - the sensors placed near the outer side of the transformer gap. In Figure 3.2, there is shown dismantled transformer with the rubber gasket inside a gap between the top and bottom transformer tank.

Fig. 3.2: Dismantled transformer with rubber gasket inside the gap

When a partial discharge occurs in the transformer tank, it will produce an electromagnetic wave in the form of an impulse-like signal, shown in Figure 2.9a. The impulse waveform has a nanosecond duration and a corresponding frequency content in the ultra-high frequency range. The electromagnetic wave propagates from the location of the PD occurrence to a transformer joint gap. Such gaps can be found in many locations around the transformer's tank. Typical is a circumferal joint gap between the upper and bottom parts of the tank. The significant fact is that the joint is not usually realised as a tight metal to metal connection. There is a gap between the metal parts, and it is filled by a dielectric gasket to prevent an oil leak. Therefore, it represents a place where the electromagnetic wave generated by PD can exit the transformer tank. It creates conditions similar to the propagation of electromagnetic waves between two parallel conducting planes. This process causes the leakage of these waves through the transformer gap. In the back section of the gap, diffraction occurs. This process is shown in Figure 3.3.

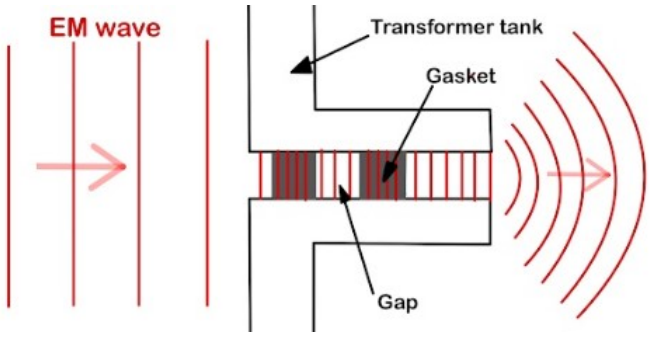

Fig. 3.3: Diffraction of the propagating electromagnetic wave through joint gap of the transformer tank

There is a known influence of the gap height and depth on the propagation characteristics of the electromagnetic wave [19]. The simulation results within the gap are shown in Figure 3.4.

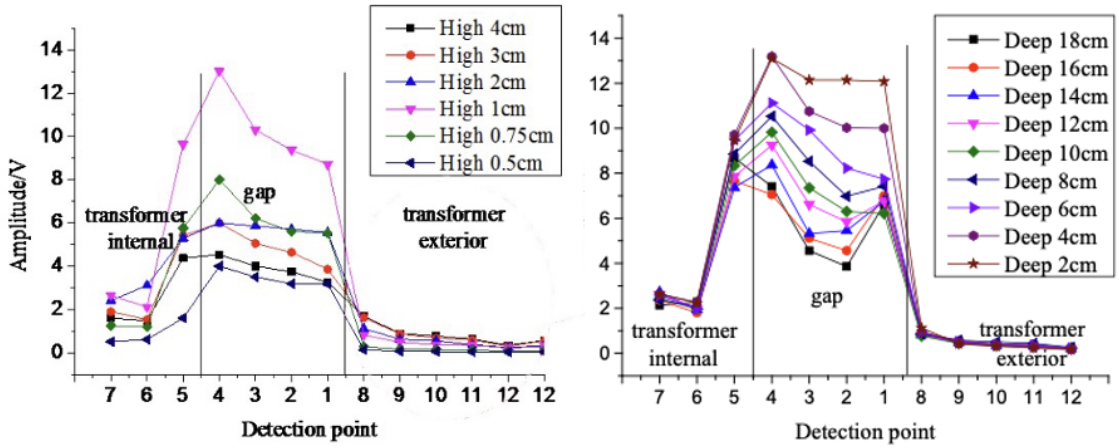

Fig. 3.4: Influence of gap height (left side) and depth (right side) on propagation characteristics of the PD electromagnetic waves [19]

The intensity of propagating signal firstly increased, in the middle of the gap reached the maximum, and in the exterior of the transformer decreased. The highest intensity of the electromagnetic wave was shown when the gap in the simulation is one centimetre high. In Figure 3.4 there are shown the simulation results in a gap with a height of one centimetre and different depths. The characteristics have a similar behaviour; however, the maximum intensity occurs in the entrance and at the end of the gap. The mentioned study analysed the distribution of electromagnetic waves through gaps with different heights and depths. According to the study, the

intensity of the electromagnetic field is significantly higher inside the gap. For that reason, the sensor should be inserted inside the gap to improve the sensitivity [19].

The amount of leaked signal is related to the dimension of the gap and the frequency of the signal. The simulations in [19] proved that there is the possibility to measure the electromagnetic wave outside the transformer tank due to the leakage of the signal through the gap. The gap behaves as two parallel conductive plates, and the signal is able to escape owing to reflections from them. Due to these successful measurements, in the next chapter, an effort is made to design our UHF external sensor.

4 Design of sensor

Between the upper and lower parts of the transformer tank, there is the gap already mentioned. It is usually filled with a rubber gasket. Despite a certain attenuation, the outer sensor can detect the partial discharge signal in the gap. There is the possibility of spreading the electromagnetic signal through the gap. The gap represents two conductive parallel plates. This structure behaves as a waveguide.

Despite the fact that the waveguide has a really short wavelength, it defines the specific arrangement of the electric and magnetic fields. It is necessary to consider this in the design of the external sensor to reach the highest possible efficiency in receiving the signal that leaks from the gap. To fulfil the requirement, there are waveguide-to-coax adapters, which will be explained in Section 4.4 Waveguide-to-coax adapter. Design with an appropriate position of the probe in the adapter can lead to maximum use of the electromagnetic field and boost the sensitivity of the sensor. The transverse dimensions of the adapter should be matched with the dimensions of the apparatus by which the signal leaks out of the transformer tank. The waveguide-to-coax adapter should also ensure isolation from external disturbances. In Figure 4.1, there is shown an example of the gap in the transformer tank used in a power plant.

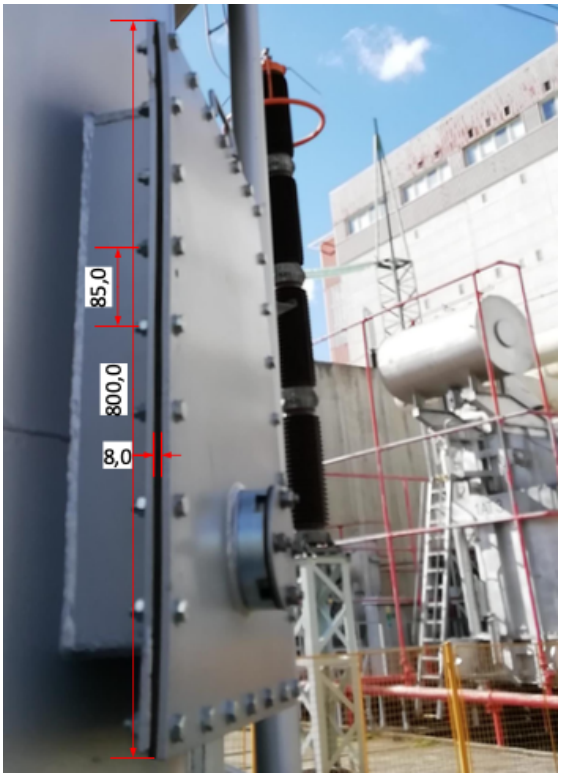

Fig. 4.1: The gap in the transformer tank. The dimensions are only for information

4.1 Waveguides

In general, a waveguide is a hollow conductive metal pipe that carries high-frequency radio waves. This metallic structure restricts the electromagnetic waves, so they propagate only inside the tube due to internal reflections from the walls. Unlike coaxial cables, there is no centre conductor inside the waveguide. The waveguide carries signals only above a certain frequency, known as **cut-off frequency**. Most of the energy below the cut-off frequency is attenuated. In summary, the waveguide acts as a high-pass filter. Each waveguide has its cut-off frequency according to its dimension. There are different types of waveguide: metallic waveguides, dielectric waveguides, parallel plates waveguides and rectangular waveguides.

Two parallel conductive plates would have an infinite cut-off frequency. But in addition to the gasket, the top and bottom parts of the transformer are joined together with the bolts. They create a rectangular cross-section and define the dimension of the waveguide. In Figure 4.2, there is a picture of a transformer tank with the gap. The designed waveguide should fit into this gap and a calculation will be made for its dimensions.

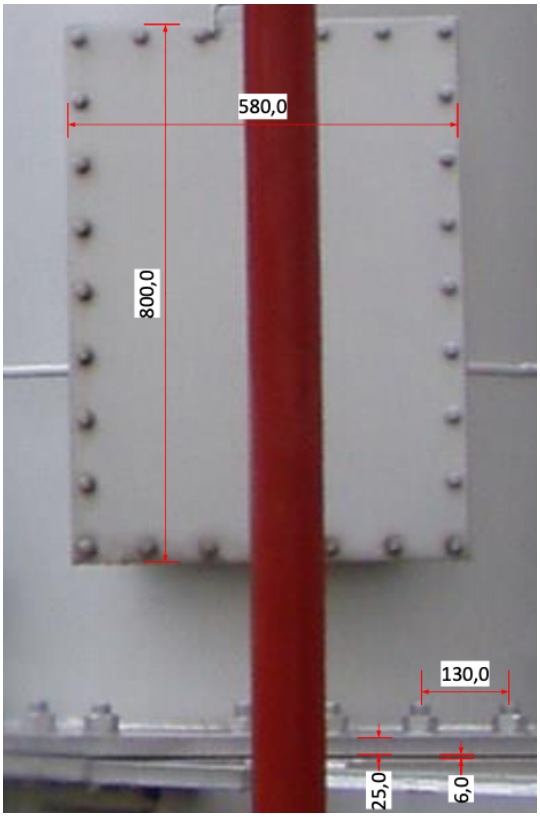

Fig. 4.2: Gap in the transformer tank. The dimensions are used for calculation in the design of the waveguide

4.2 Rectangular waveguides

A rectangular waveguide is typical for a rectangular cross-section and is defined by its dimensions: width a and height b . The width of a rectangle is usually twice as big as the height. There are some advantages of the rectangular waveguide, such as a wide frequency bandwidth for single-mode propagation and low attenuation.

The total reflection inside the rectangular waveguide results in an electric or magnetic field in the direction of propagation. In the rectangular waveguide, there are only two possible modes: TE and TM modes. TEM mode is not supported in the waveguide. TE represents transverse electric mode, which means that the electrical field is transverse to the direction of propagation. Moreover, simultaneously, this mode does not have a longitudinal component of the electric field. Transverse electric waves are also called H waves. In the transverse magnetic (TM) mode, the magnetic vector is transversal to the direction of propagation, and this mode simultaneously does not have a longitudinal component of the magnetic field. Transverse magnetic waves are also called E waves.

There are different types of propagation modes, TE and TM. Attached integers m and n to the TE or TM terms represent different wave modes, such as $\mathbf{TE}_{m,n}$ and $\mathbf{TM}_{m,n}$. The integer m indicates the number of half-waves in the long direction of the waveguide a and n represents the number of half-waves in the short direction b of the waveguide. In the rectangular waveguide, the dominant mode is the $\mathrm{TE}_{1,0}$ mode, which means that it has the lowest cut-off frequency. It is shown in Figure 4.3.

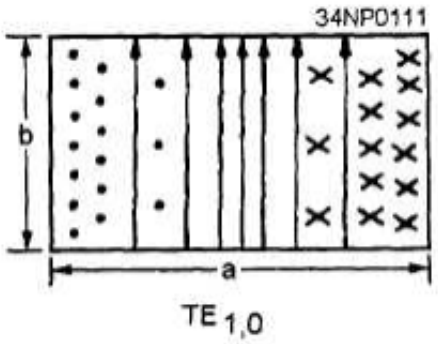

Fig. 4.3: The dominant mode $\mathrm{TE}_{1,0}$ in rectangular waveguide: in the middle of waveguide is the strongest electric field and near the walls of the waveguide is the strongest magnetic field.

In section 3.2 External UHF sensors, there was mentioned the external type of PD UHF sensor. The gap in the transformer tank acts as a waveguide. It carries

only the electromagnetic waves with a frequency above the cut-off frequency; the rest of them are attenuated. To calculate the **cut-off frequency $\mathbf{f}_c$** of the rectangular waveguide, there is the equation 4.1. The parameter a is the length and b is the width of the rectangle, and the integers m and n define the propagation mode. The cut-off frequencies of both TM and TE modes are

$$f_{c_{m,n}} = \frac{1}{2 \cdot \pi \cdot \sqrt{\varepsilon \cdot \mu}} \cdot \sqrt{(\frac{m \cdot \pi}{a})^2 + (\frac{n \cdot \pi}{b})^2} \tag{4.1}$$

For the calculation of the waveguide cut-off frequency for the external PD detector placed on the transformer gap is used the dominant mode $TE_{1,0}$ mode. This means that m equals 1 and n equals zero, and therefore the width b of the gap no longer affects the cutoff frequency of the dominant $TE_{1,0}$ mode. Consequently, the equation is simplified to the new form 4.2:

$$f_{c_{1,0}} = \frac{1}{2 \cdot a \cdot \sqrt{\varepsilon \cdot \mu}} \tag{4.2}$$

The speed of light in the free space is defined as

$$c_0 = \frac{1}{\sqrt{\varepsilon_0 \cdot \mu_0}}. \tag{4.3}$$

If the gap was filled with vacuum or air, the root expression can be substituted for the speed of light from equation 4.3, and equation 4.2 can be rewritten as

$$f_{c_{1,0}} = \frac{c}{2 \cdot a} \tag{4.4}$$

In Figure 4.2, there is the transformer tank, the tank and the base are joined to each other by bolts. The distance between two bolts represents the length of the waveguide and the expected value is around 130 millimetres.

The gap was filled with vacuum or air, the cut-off frequency of the designed waveguide will be

$$f_{c_{1,0}} = \frac{2,998 \cdot 10^{-8}}{2 \cdot 0,130} = 1.15GHz$$

4.3 Waveguide couplers

Waveguide couplers are equipment that distributes energy in or removes energy from the waveguides. There are three types of waveguide couplers: probe, loop and apparatus. The apparatus may also be called slots or windows. In the waveguide, there is a small slot and the energy penetrates the waveguide through it. It uses diffraction, and as electromagnetic waves enter the waveguide, they expand across the whole waveguide. The location of slots influences which type of field is used for waveguide excitation mode, which is shown in Figure 4.4. This method is used only when the other two are inefficient. The other types of waveguide couplers will be discussed in more detail in the following sections.

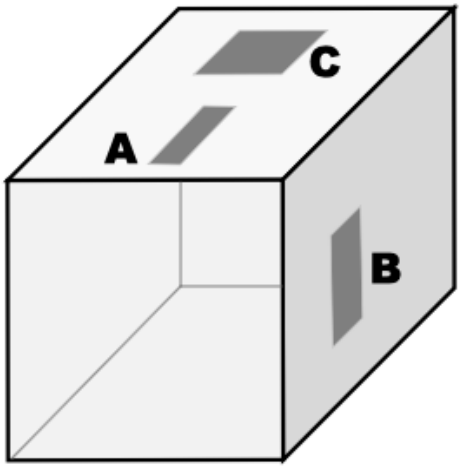

Fig. 4.4: Slot coupling. Slot A is used for electric coupling and is at the maximum of the electrical field. Slot B is used for magnetic coupling and is at maximum of the magnetic field and slot C is at maximum of both E and H field and is a form of electromagnetic coupling

4.3.1 Current probe

In the case of a probe coupling, a center conductor of a coaxial cable probe is inserted into the waveguide. This probe behaves as a monopole probe. The second pole is replaced by a conductive plane represented by a wall of the waveguide. The configuration of the current probe coupler is shown in Figure 4.5.

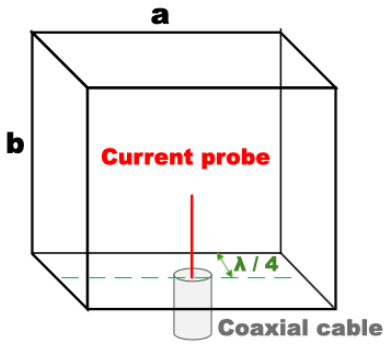

Fig. 4.5: The setup of current probe setup

In the case of injecting energy into the waveguide, the current flows in the probe and sets up the electric field. Subsequently, the probe radiates this energy in the form of E waves into the waveguide. In the opposite case, the E waves with perpendicular magnetic waves induce a current in the probe. The most efficient place to place the

probe is the centre of the longer side of the waveguide (length) a and one quarter-wavelength $\lambda_g/4$ from the shorted end of the waveguide. In one-quarter of the wavelength, there is the maximum of the dominant $TE_{1,0}$ mode. The dimension of the quarter-wavelength depends on the frequency of the waves that are required to be received or radiated.

4.3.2 Loop probe

In the case of a loop probe, a coaxial cable probe is formed in the loop. It uses a magnetic field. In the case of putting energy into the waveguide, the current flows in the loop and sets up the magnetic field. In the case of receiving energy, the magnetic field in the waveguide induced the current in the loop.

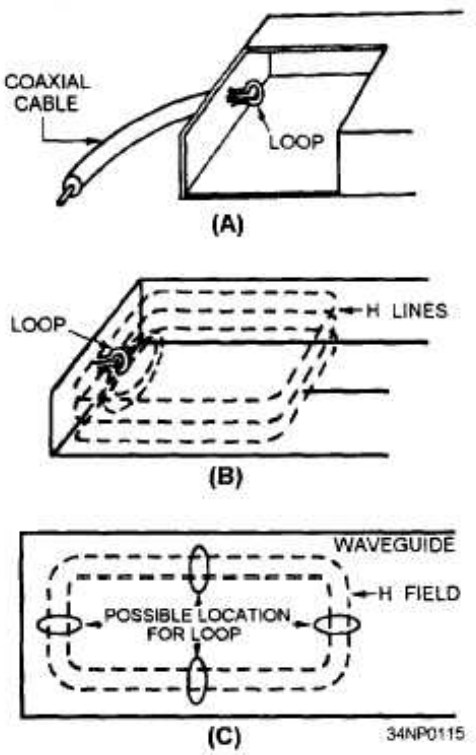

Fig. 4.6: The explanation of loop coupling: A) loop formed from coaxial cable probe, B) maximum intensity of M waves C) best theoretical positions for placing the loop [23]

In Figure 4.6, there are illustrated four options to place the loop in a waveguide to use the greatest strength of M waves and magnetic field. The centre of the loop should be in the middle of the shorter dimension of the waveguide (height) b.

4.4 Waveguide-to-coax adapter

The probe and loop couplers discussed above are important parts of the waveguide-to-coax adapters. When a partial discharge occurs in the transformer tank, the emitted electromagnetic waves are scattered in many directions. They strike a gap, leak out of the tank through the mentioned gap and enter the mounted waveguide part of the external sensor. This energy of the electromagnetic field is transformed into an electrical signal which is then sent through the coaxial cable connected to the signal processing and evaluation equipment, such as an oscilloscope or digitizer and computer. In our design, two options will be discussed and researched: the function and efficiency of probe and loop couplers in the waveguide-to-coax adapters.

4.4.1 Probe coupling

As discussed in the previous section, the specification of a certain location of the coaxial cable probe is important to achieve maximum intensity and sensitivity. The best theoretical position for a monopole probe is in the middle of a waveguide width and one-quarter of the guided wavelength λ_g from the shorted end of the waveguide. The wavelength is specific for each waveguide and depends on the dimensions and modes of the waveguide, specifically, the integers m and n.

The guide wavelength λ_g is the distance through which the wave with phase velocity v_f passes through the waveguide in the period of the signal $T = 1/f$. The guide wavelength is defined as:

$$\lambda_g = \frac{\lambda}{\sqrt{1 - (\frac{\lambda}{\lambda_m})^2}} \tag{4.5}$$

where λ_g is the guide wavelength, λ_m is a cut-off wavelength and λ is the free space wavelength. By replacing the wavelength with the expression $\lambda = c/f$, the expression can be rewritten as:

$$\lambda_g = \frac{\frac{c}{f}}{\sqrt{1 - (\frac{\frac{c}{f}}{\frac{c}{f_m}})^2}} \tag{4.6}$$

The cut-off frequency f_m, with dominant $TE_{1,0}$ mode and length a 130 mm, is $\lambda = 1.15GHz$. This cut-off frequency is typical for the rectangular waveguide size WR510/WG7/R18. The recommended frequency band of this waveguide is between 1.45 and 2.20 GHz. The centre of this frequency band, λ = 1.825 GHz, which

still belongs to the UHF range, will be used for the calculations. The waveguide wavelength λ_g is equal to

$$\lambda_g = \frac{\frac{3 \cdot 10^8}{1.825 \cdot 10^9}}{\sqrt{1 - (\frac{\frac{3 \cdot 10^8}{1,825 \cdot 10^9}}{\frac{3 \cdot 10^8}{1.15 \cdot 10^9}})^2}} = 211\, mm$$

.

This means that the monopole probe in the designed waveguide should be λ_g / 4, that is, **53 millimetres**, away from the shorted end.

4.4.2 Material of the designed waveguide

The waveguide adapter will be located in the environment with a presence of strong electromagnetic disturbance. So the construction of the waveguide needs to have a strong immunity to outer disturbances. For the test in a laboratory, the designed waveguide adapter will be made up of the PCB board, that will be soldered together due to easy construction that will be sufficient for experimental verification. The PCB boards are usually produced from FR-4, which is a flame-retardant epoxy resin and glass fabric composite. FR-4 is a plastic material with good mechanical and electrical insulating materials.

5 Simulations

5.1 Model in Ansys HFSS

Ansys HFSS (high-frequency structure simulator) is a 3D electromagnetic simulation software for designing and simulating high-frequency electronic products, such as antennas and waveguides. In this bachelor thesis, the software is used to verify the high-frequency behaviour of the waveguide-like apparatus mentioned in Chapter 4. The results of the presented simulations will be used for the sensor design and manufacture. The main goal is to track the intensity of an electric and magnetic field and the attenuation of the leaking electromagnetic signal.

The model is shown in Figure 5.1. On the left side, there is the original model that includes bolts (parts with a dark grey colour) and the metal material that borders the air inside the waveguide-like apparatus (parts are light grey). On the right side is the simplified model, which includes only air. For further simulations, it will be used the simplified model. The thickness of the real material is inappreciable, so the discussed parameters of the simplified model will be considered as parameters of the real designed one. The parts with green colour are the gaskets, which are defined as rubber material. For simulations, it is important to define the boundaries that define the solution space. All walls (except the wave port, which will be explained later) were defined as *PEC, perfect electrical conductor*. On the back side, there is the waveport, which determines the area where energy enters the adapter. It is marked in red in Figure 5.1b.

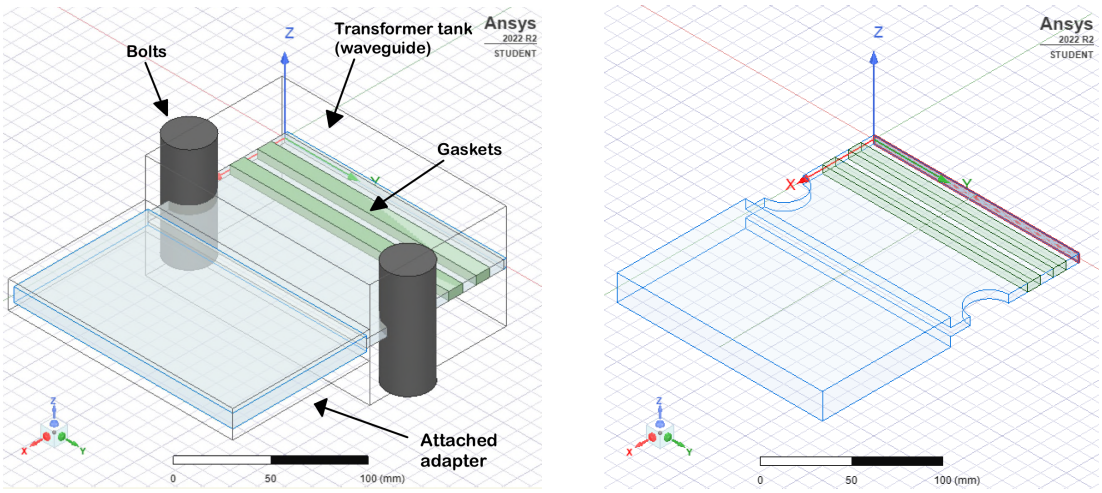

(a) Original model

(b) Simplified model

Fig. 5.1: Isometric view of the original and simplified model used for simulations

5.2 Electromagnetic field distribution

The software is a 3D electromagnetic solver based on the finite element method. There are different types of solution options. But for the design, it was used Direct Solver and also the possibility of field overlays, provided magnitude or vector mapping of the electric and magnetic fields. At the same time, the ability to process the data into 2D or 3D graphs was used. The wave port was set to generate the electromagnetic wave in the $\mathbf{TE}_{1,0}$ mode with the cut-off frequency, that is, 1.15 GHz, and then at a frequency above this limit. For this experiment, it was chosen the 1.5 GHz frequency.

5.2.1 Electric field

In Figure 5.2, there are shown the differences in the propagation of the electric field when the EM signal has the cutoff frequency **1.15 GHz** and the selected **1.5 GHz** frequency. Furthermore, inside the sensor with different heights of its casing. The EM wave with the cut-off frequency is significantly more attenuated within the sensor body than the EM wave with a higher frequency. For frequencies above the cut-off frequency, there is evidently less attenuation. The dimensions of the waveguide-like apparatus were calculated from the available sources and images. The width of the waveguide-like adapter and sensor is given by the distance of the bolts that join the upper and lower parts of the transformer vessel. The assumed value is 130 millimetres. The other parameters, height and length, are variable and can be modified.

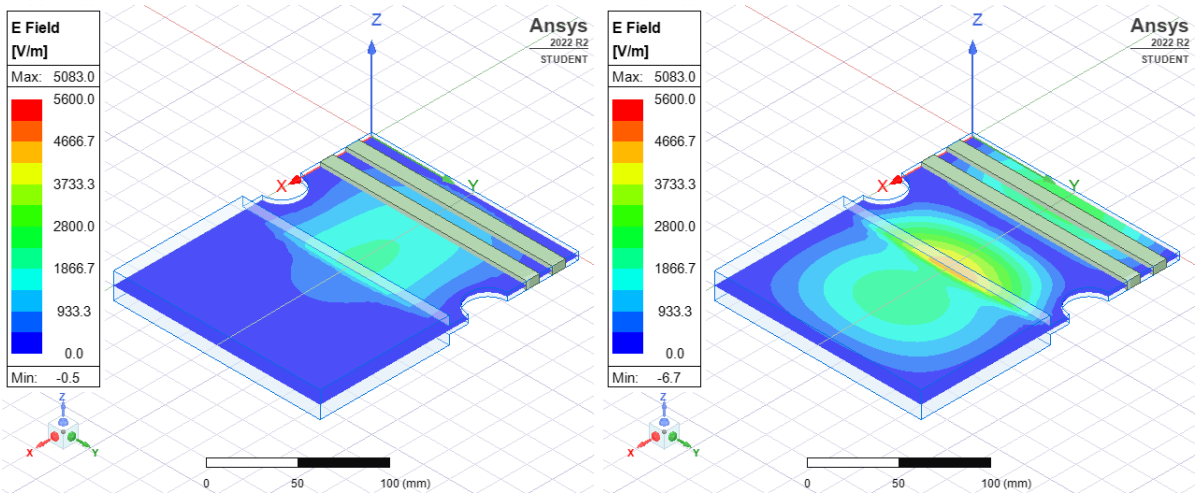

(a) 1.15 GHz frequency and 20 mm sensor (b) 1.5 GHz frequency and 20 mm sensor

Fig. 5.2: An electric field displayed for 1.15 GHz and 1.5 GHz wave frequency and different height of the sensor casing

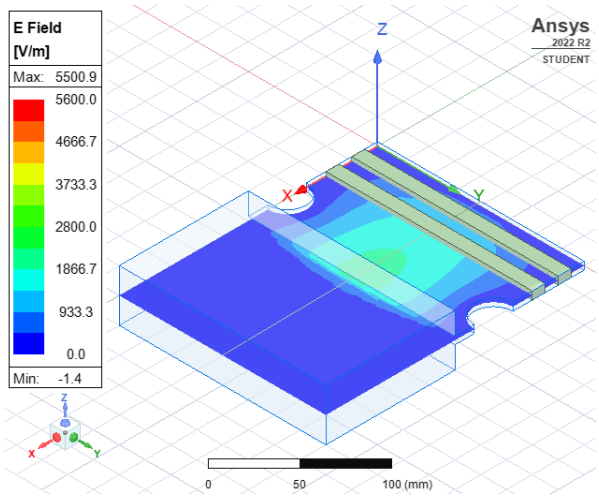

(c) 1.15 GHz frequency and 40 mm sensor

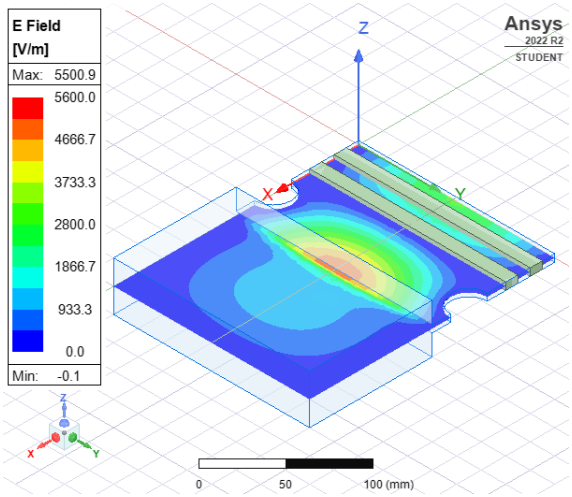

(d) 1.5 GHz frequency and 40 mm sensor

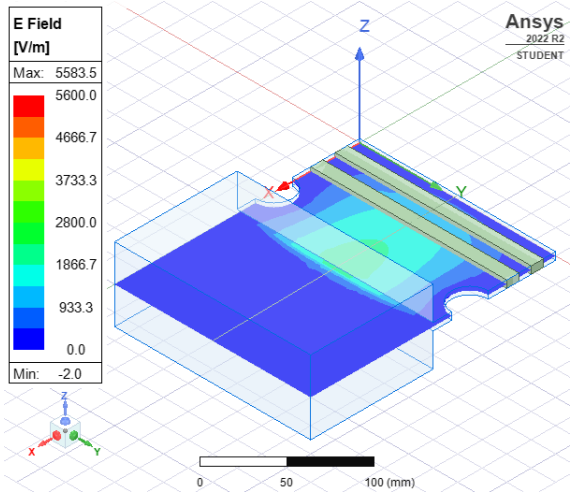

(e) 1.15 GHz frequency and 60 mm sensor

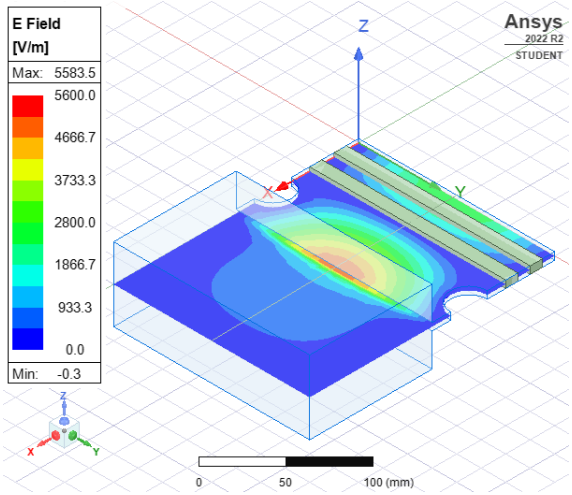

(f) 1.5 GHz frequency and 60 mm sensor

Fig. 5.2: An electric field displayed for 1.15 GHz and 1.5 GHz wave frequency and different height of the sensor casing

The analyse evaluates the intensity of the electric field, depending on the height and length of the sensor. Its results are shown in Figure 5.3. On the y-axis is the height of the adapter and on the z-axis there is the intensity of an electrical field. On the x-axis, there is the distance from the interface between the inner wall of the transformer tank and the gap exit, explained in Chapter 4. The length of the adapter is 100 mm, and after that, there is placed the external sensor with the same length. The most obvious attenuation occurs at the moment the wave reaches the level of 100 mm distance, which is the area of connection of the transformer gap and the sensor. Moreover, the height of the attached waveguide-to-coax sensor has a considerable influence on the already enormous attenuation of the spreading signal.

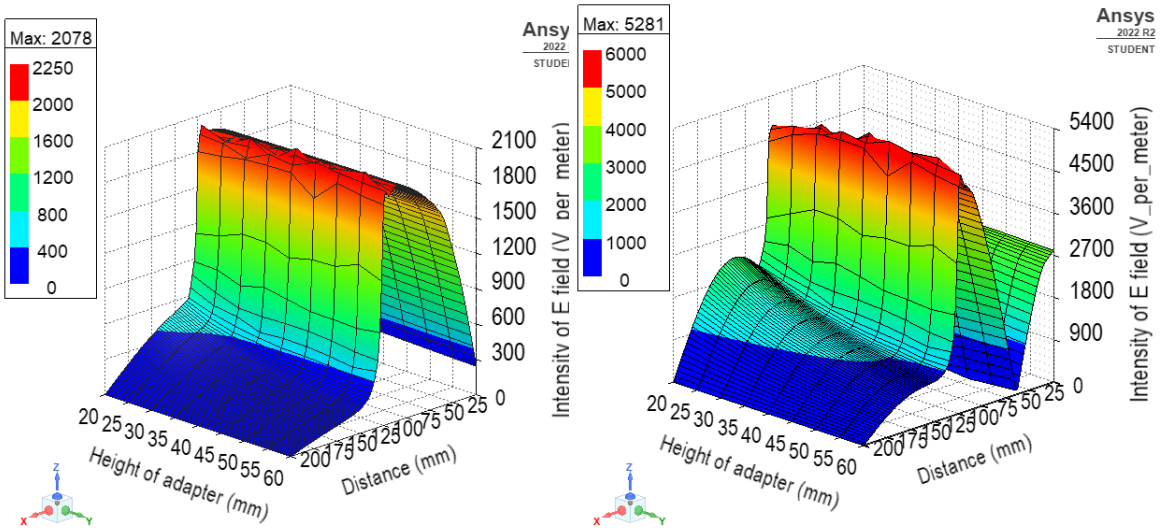

(a) Wave with 1.15 GHz frequency

(b) Wave with 1.5 GHz frequency

Fig. 5.3: 3D graph of a relationship between the intensity of the electrical field, the distance from the source of EM wave and the height of the attached sensor

Knowledge of the E field distribution is important for the correct design of the external sensor with probe coupler, explained in Section 4.3.1. The best solution will be **the adapter with 130 mm width, 100 mm length and 20 mm height**.

The behaviour of the sensor was also tested for 20 mm sensor casing and other frequencies. The E intensity is lower for these frequencies. The results of the test are shown in Figure 5.4.

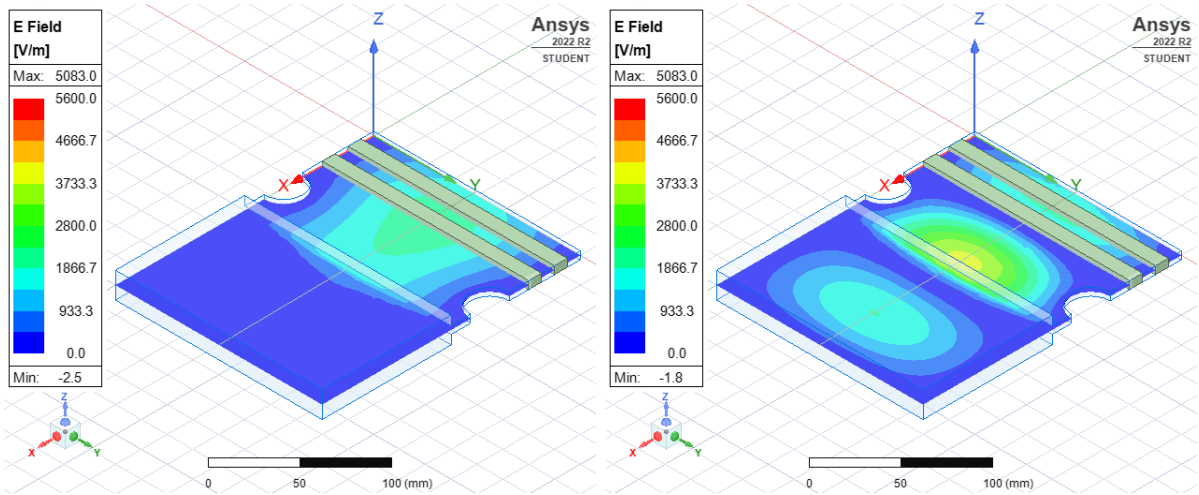

(a) 1 GHz frequency

(b) 2 GHz frequency

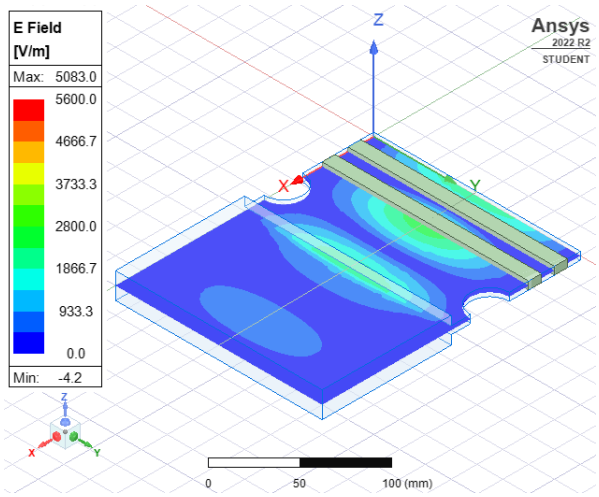

(c) 2.5 GHz frequency

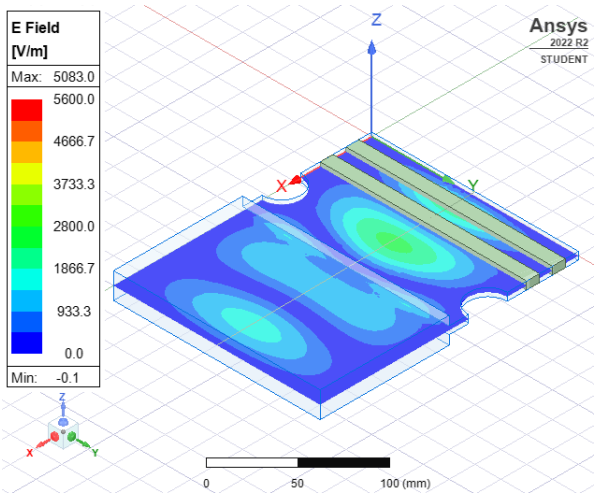

(d) 3 GHz frequency

Fig. 5.4: An electric field displayed for 1 GHz, 2 GHz, 2.5 GHz and 3 GHz wave frequency and 20 mm height of the sensor casing

5.2.2 Magnetic field

The identical tests were computed for the magnetic component of the EM field. The width of the waveguide-like adapter remains 130 mm. The other parameters, height and length, can be modified. In Figure 5.5, there are shown the examples of different behaviour of the magnetic component of EM field for the cut-off frequency **1.15 GHz** and the selected **1.5 GHz** frequency, and for various heights of the sensor.

The EM wave with the cut-off frequency is also notably more attenuated than the EM wave with a higher frequency.

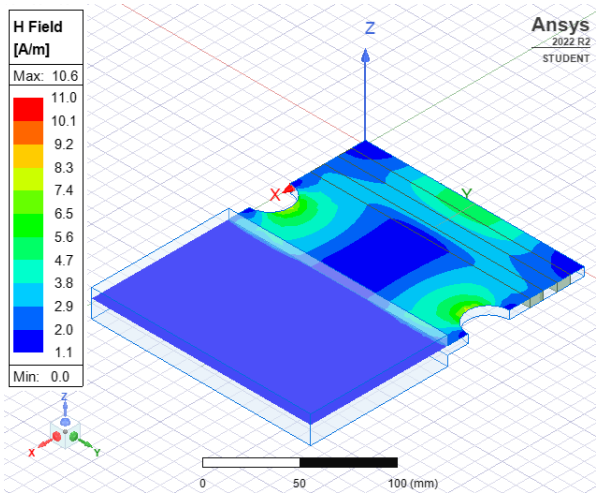

(a) 1.15 GHz frequency and 20 mm sensor

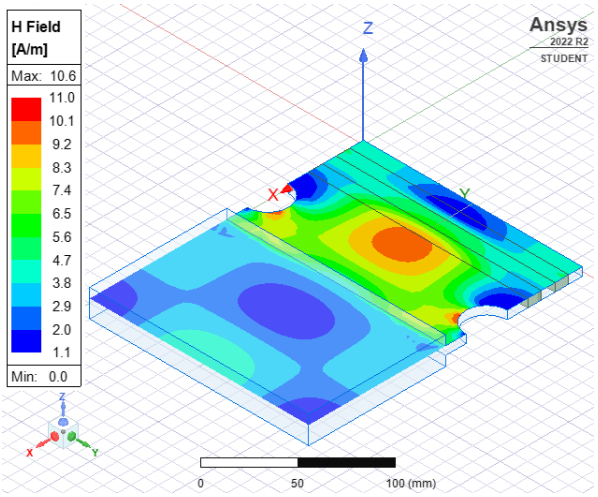

(b) 1.5 GHz frequency and 20 mm sensor

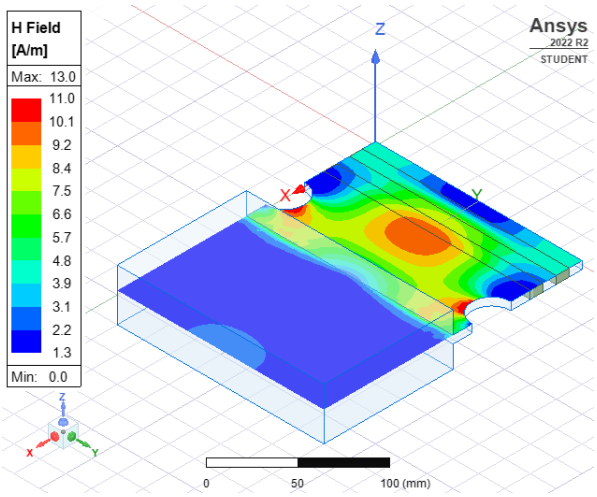

(c) 1.15 GHz frequency and 40 mm sensor

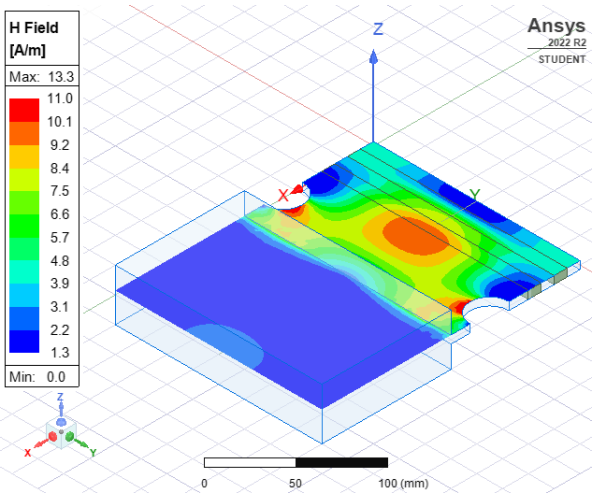

(d) 1.5 GHz frequency and 40 mm sensor

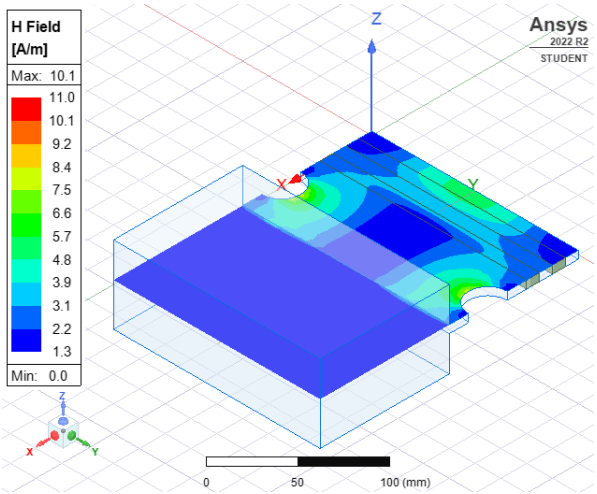

(e) 1.15 GHz frequency and 60 mm sensor

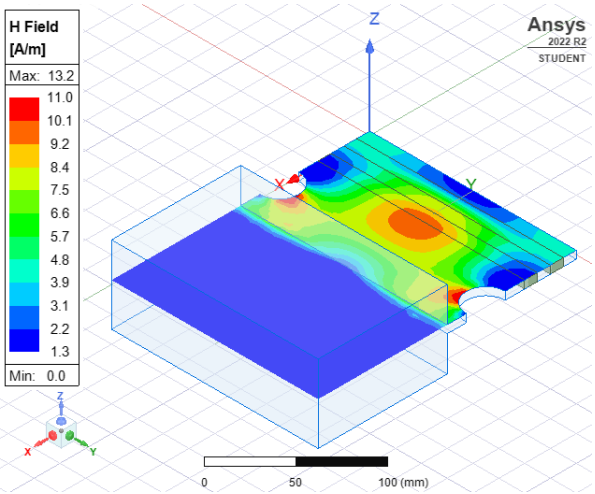

(f) 1.5 GHz frequency and 60 mm sensor

Fig. 5.5: A magnetic field displayed for different variations of wave frequency and height of the sensor casing

The magnetic field behaves in the same way as the electric field. The intensity H changes depending on the distance from the source of the EM waves and the height of the sensor. The graphs of the function of magnetic intensity H of the EM field, distance from the source and height of the sensor are shown in 5.6.

In the test, there is a different form of an obvious attenuation of the intensity of a magnetic field. The largest difference is at the end of the attached sensor. For the magnetic field of $\mathbf{TE}_{1,0}$ mode is typical that the maximum of the magnetic field is in the middle of the boundaries (back and side wall of the adapter) of the waveguide, which can be seen most clearly in Figure 5.5b.

The results of the H-field distribution for different distances and heights will be

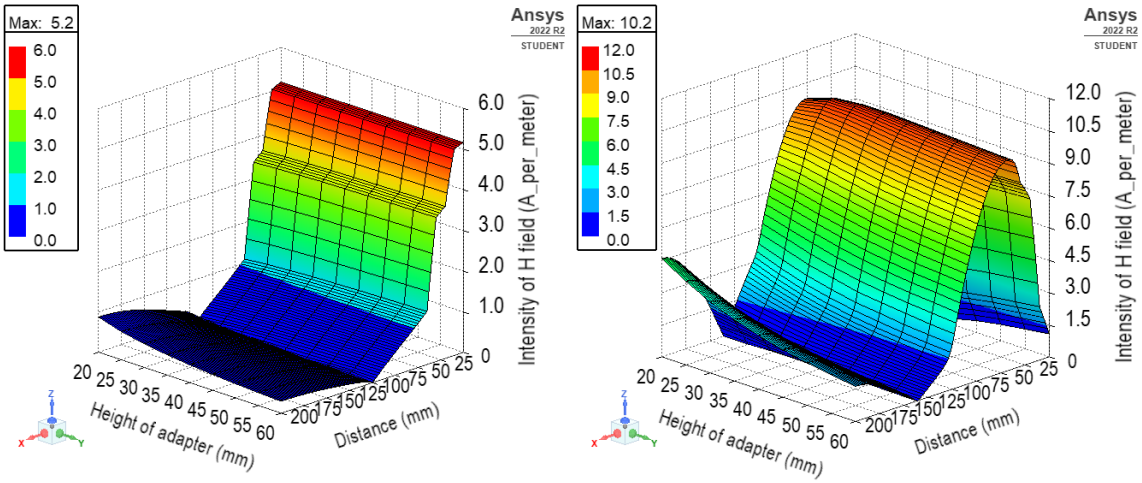

(a) Wave with 1.15 GHz frequency

(b) Wave with 1.5 GHz frequency

Fig. 5.6: 3D graph of a relationship between intensity of a magnetic field, distance from the source of EM wave and the height of the attached adapter

used for the sensor design. For sensing the magnetic field, in Section 4.3.2, loop coupling was mentioned. A small loop will be placed on the back side of the sensor and in the middle of the width of the sensor. The simulations of a magnetic field have the same results. The best solution for the implementation will be the sensor with **130 mm width, 100 mm length, and 20 mm height**.

The magnetic field was also tested for the distribution of the signal with frequencies: 1 GHz, 2 GHz, 2.5 GHz and 3 GHz. It can be seen that the magnetic intensity is lower for these frequencies. The results of the test are shown in Figure 5.7.

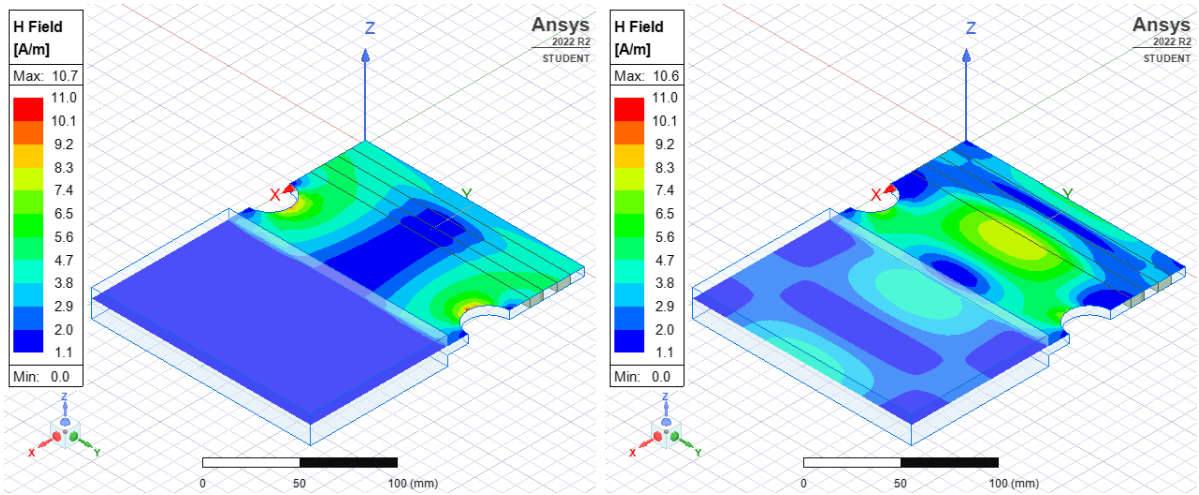

(a) 1 GHz frequency

(b) 2 GHz frequency

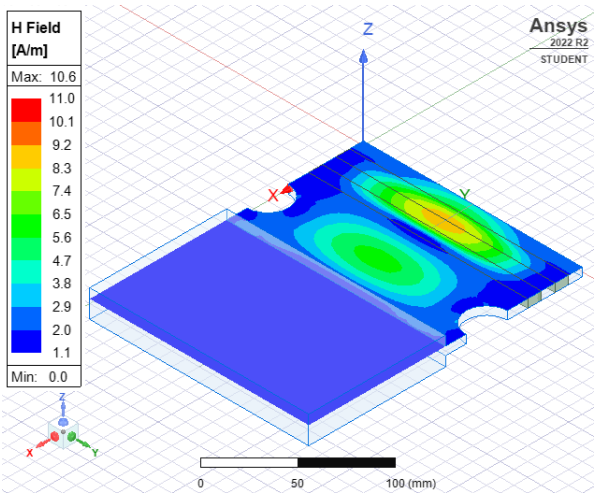

(c) 2.5 GHz frequency

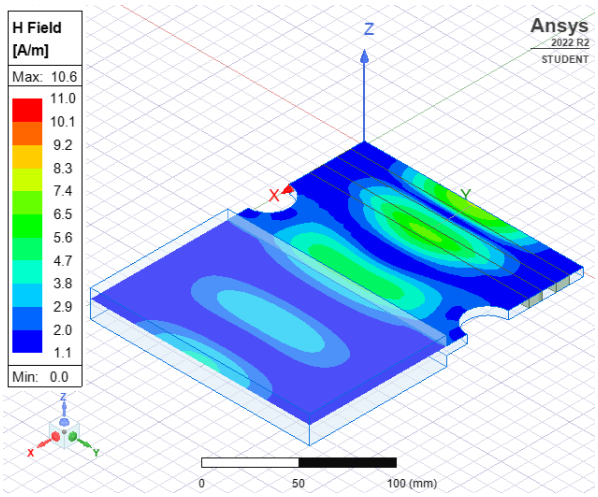

(d) 3 GHz frequency

Fig. 5.7: A magnetic field displayed for 1 GHz, 2 GHz, 2.5 GHz and 3 GHz wave frequency and 20 mm height of the sensor casing

5.3 Results of simulations

To sum up all the results of the simulations, on the surface between two different components, transformer gap and the sensor, there will be a considerable attenuation of the energy of the EM waves. Based on this negative fact, it is necessary to choose the best dimensions. Both of the EM field-signal coupling methods were chosen for the experimental sensor realization, in order co compare their properties and sensitivity. The first one will measure the intensity of the electric field and will be based on the probe coupling.

For maximum extraction of the energy of partial discharge, the sensor should be 130 mm wide, 100 mm long, and 20 mm high. Figure 5.8 shows the vector distribution of the E field. This value was chosen because it is the frequency above the cut-off frequency 1.15GHz. Also signal with this frequency has the smallest attenuation in contract to other tested frequencies. The maximum of the electric component of EM field inside the sensor for the 1.5GHz frequency is 60 mm from the back side for 1.5GHz frequency. The value was identified with simulation, but is connector with Equations explained in Section 4.3.1.

The second one will use the principle of loop coupling and will be sensed to the magnetic component of EM field. The vector distribution of the magnetic field is shown in Figure 5.9. The pick-up loop probe will be placed on the back side of the sensor. In Figure 5.9b, this area is light blue and the plane of the loop should be perpendicular to the direction of the magnetic field to maximise the value of the induced current in the loop. For less attenuation, the sensor will have the same

dimensions as the first one with probe coupler, which means 130 mm width, 100 mm length, and 20 mm height.

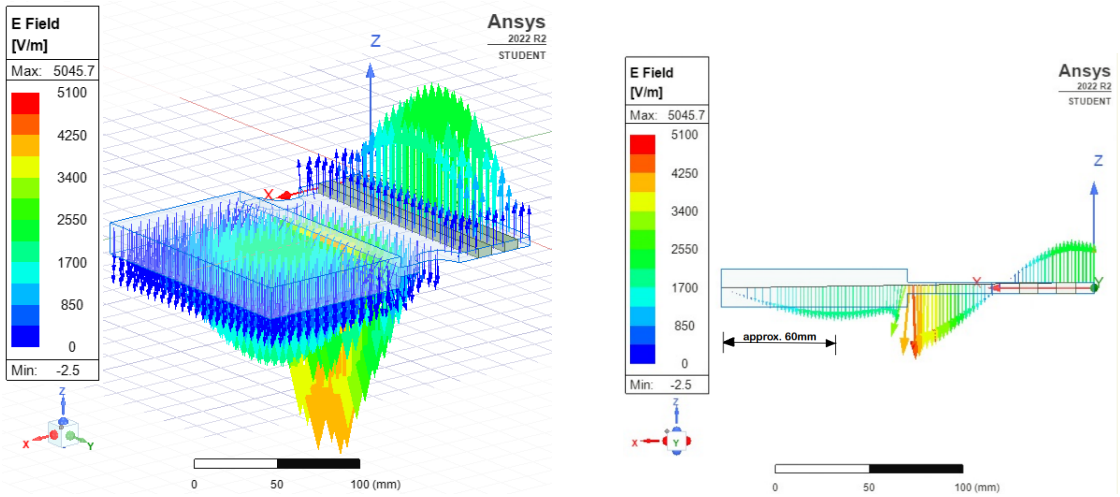

(a) Isometric view (b) Left view

Fig. 5.8: Vector distribution of the electric field for 1.5GHz frequency and 20 mm sensor casing

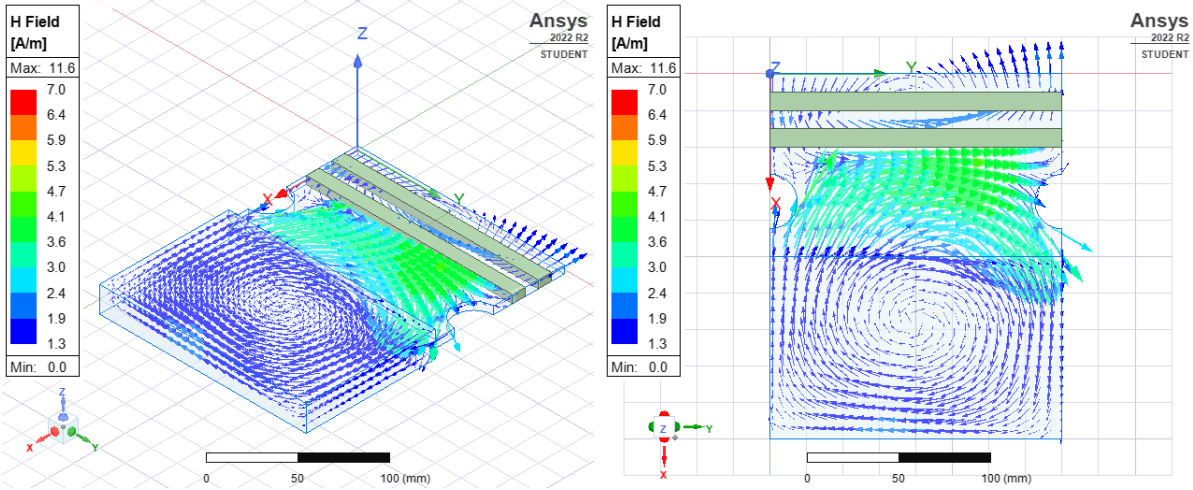

(a) Isometric view (b) Top view

Fig. 5.9: Vector distribution of the magnetic field for 1.5GHz frequency and 20 mm sensor casing

6 Construction of external PD UHF sensor

6.1 Simplification of simulated model

There was an effort to simplify the production and analysis process, especially a model that represents the structure around the transformer tank gap. The model of the mentioned structure is shown in Figure 5.1a and can be replaced by a metallic plate, which will shield the entrance of the waveguide-to-coax adapter. So it is not necessary to manufacture a model that represents the structure around the transformer tank gap. The metallic plate will have a slit in the middle, which represents the interface between the transformer tank and the adapter. This simplified approach was simulated in the Ansys HFSS software to verify the behaviour of the slit. The simplified model used for the simulations is shown in Figure 6.1.

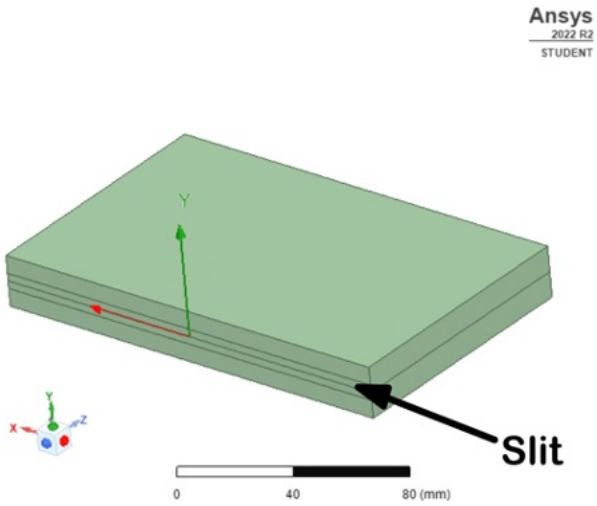

Fig. 6.1: Simplified model tested in Ansys software and used as a model for manufacture. The slit has 130 mm width and 6mm height

The simulations were performed for the 1.5GHz frequency signal. The electromagnetic wave is spreading from the outlying source, and it can be seen the process of entering energy inside the sensor. Figure 6.2 confirms that the sensor behaviour remains the same as in the case of the original, more complex, mentioned in Section 5.1. The electric field has the maximum of electric intensity in the middle of longer dimension and approximately 60 mm from the shorted end. The maximum of magnetic intensity in the middle of the longer dimension but close to the back side.

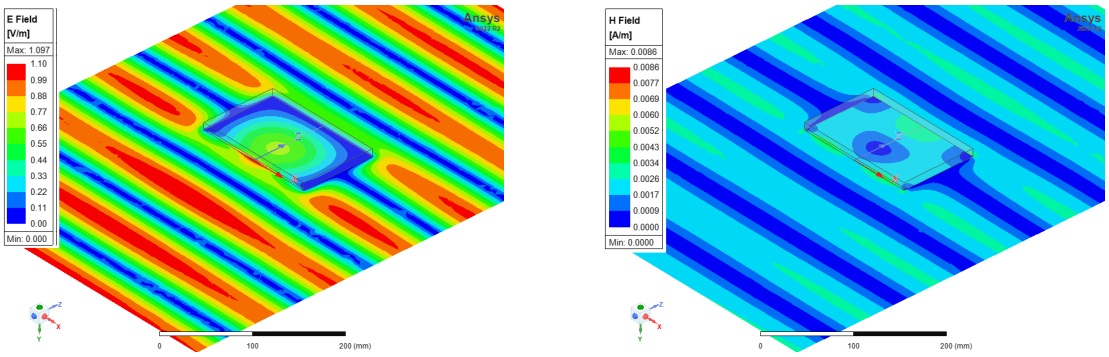

(a) Electric field (b) Magnetic field

Fig. 6.2: Simulations of the adapter to simplify the production

6.2 Construction of the sensor box

The sensor box is made of FR4 substrate plates, with a thickness of 1.55 mm, coated with a 35μm copper foil layer. The total thickness is considered to be 1.6 mm. The dimensions of each sensor wall can be seen in Figure 6.3.

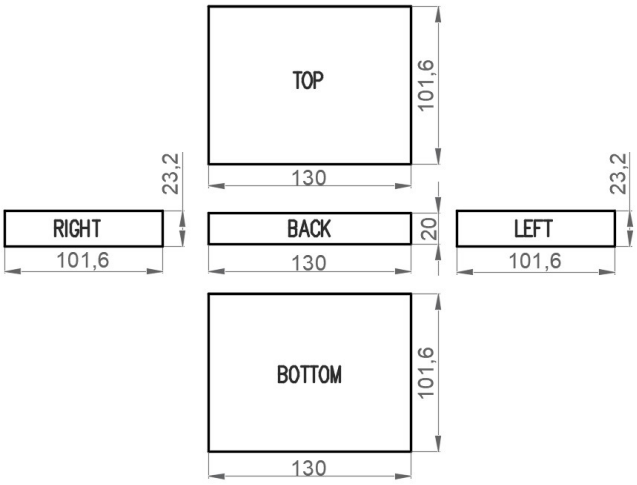

Fig. 6.3: Dimensions of plates of FR4 substrate with an one-side layer of cuprum used for sensor (the dimensions are in millimetres)

The one-sided copper plates of the designed waveguide-like sensor were overlaid with a layer of silver by means of chemical deposition. Silver has a higher electrical conductivity, which should lead to lower losses inside the waveguide. It also protects the copper layer against oxidation. The plates can be seen in Figure 6.4. In the middle of two plates, there are holes prepared to insert the monopole current and the loop induction probe.

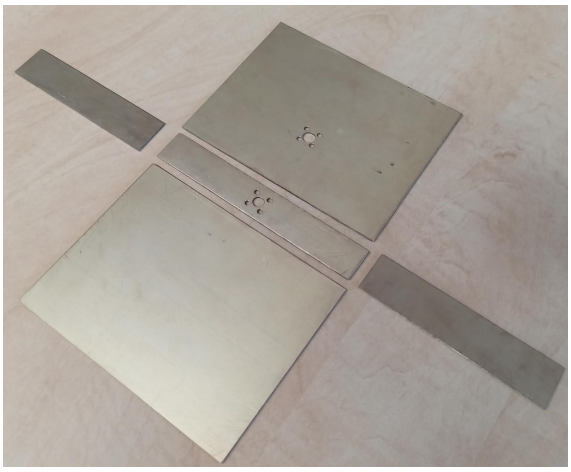

Fig. 6.4: Plates with a layer of silver used for manufacture

In the previous chapters, there were mentioned two types of waveguide couplers, which are suitable for the design of the waveguide-to-coax sensor: current probe and loop probe. The current probe coupler behaves as a monopole antenna with short electric length. The vertical electric field of the basic waveguide mode induces a current in the probe. The height of the sensor casing is quite small in comparison to wavelength of the EM wave considered for the sensor design in terms of frequency. That means, the current probe cannot have the optimal length close to quarter of the wavelength. A question arises as to whether the longest possible probe will be the best solution, since an unwanted capacitance between the probe and the sensor's wall can decrease the sensitivity. To analyse this issue, two probe lengths were proposed. They are shown in Figure 6.5a.

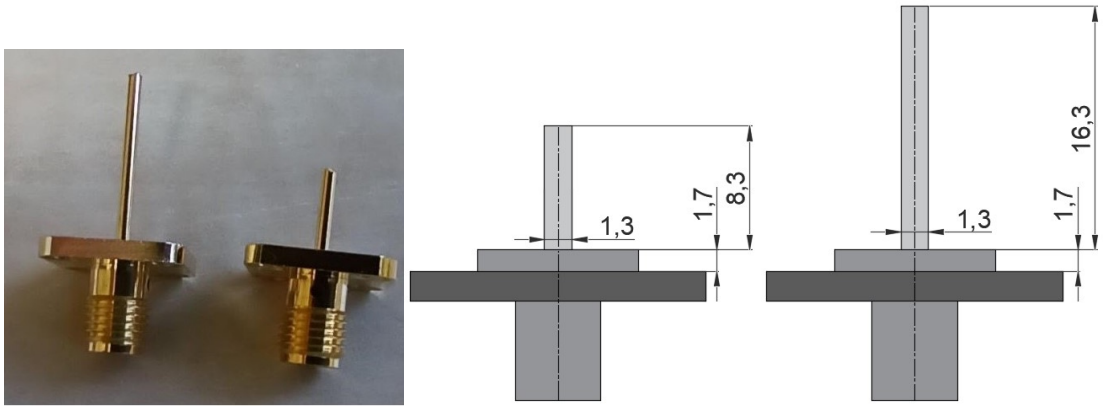

(a) Used monopole probes (b) Dimensions (in millimetres)

Fig. 6.5: The SMA connector with two length of electric field component probes

The different sizes will provide particular information on the sensitivity and behaviour of the designed sensor. The monopole probe is part of the RF SMA connector, from the manufacturer MULTICOMP PRO, Part. No MP-19-13-11-TGG. The dimensions of the monopole probes are shown in Figure 6.5b. Both monopole probes were placed on the bottom side of the adapter and 65 mm from the back side. The value was determined from the simulations shown in Figure 5.8b. It can be seen in Figure 6.6.

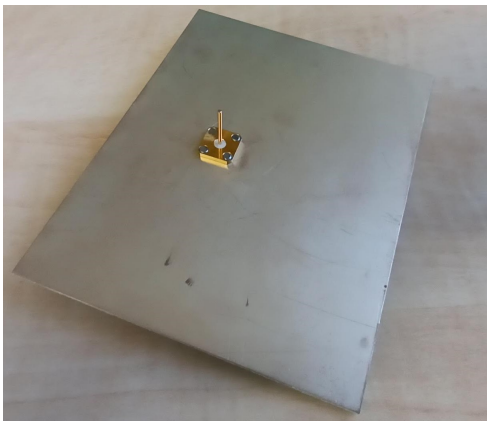

Fig. 6.6: Monopole probe fixed on the bottom side of the adapter

In the matter of loop probe, the time variable magnetic field induces a curly electric field around the loop, and the result is an electric current flowing from the loop to the coaxial cable and the input of the measuring instrument. In the same way as current probes, for the test were used two sizes of loops to compare their sensitivities and possible influence on bandwidth limitation. The loop probes dimensions and physical realization are shown in Figure 6.7a.

(a) Used loop probes

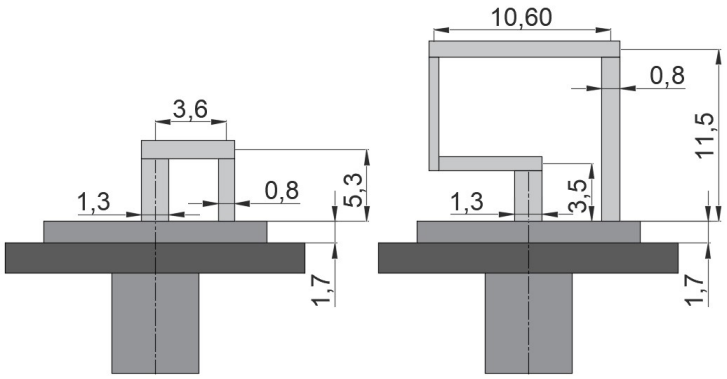

(b) Dimensions (in millimetres)

Fig. 6.7: The SMA connector with two sizes of magnetic field component probe

The dimensions of the loop probes are shown in Figure 6.7b. Both current loops were placed in the middle of the back of the sensor casing, which shows Figure 6.8. The current loop was made from the RF SMA connector from the manufacturer MULTICOMP PRO, Part. No. MC000981. The wires were then formed into the loop and soldered to the connectors.

Fig. 6.8: Current loop fixed on the back side of the adapter

The connectors are placed on the inner side of the sensor in order to provide the electrical conjunction. To have only one adapter, but with variable connector, the connectors are not soldered to the adapter. For the designed adapter was used Philips screws with countersunk head. Figure 6.9 shows the way screws were used to fix the connector to the walls.

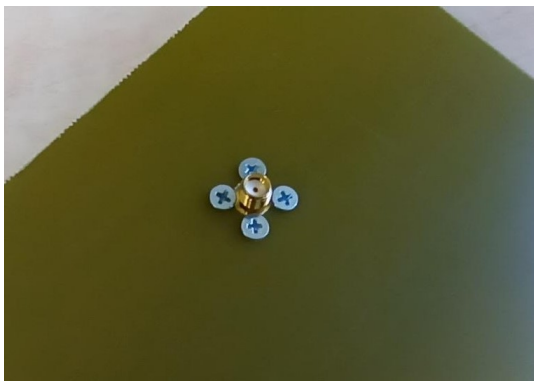

Fig. 6.9: Connectors are attached to the adapter with M3 Philips countersunk head screws

In the flange of the connector was cut the thread for the M3 screws. A countersink hole was milled on the outer side of the sensor wall to allow the head of a countersunk screw to sit flush with the surface of the surrounding material of the wall. It should prevent the screw from coming into contact with the connector of the connected cable. In the case of the need of a probe change, the screws will be unscrewed and another connector with a different probe size will be placed and fixed back with screws.

The adapter is too narrow, so it will be difficult to solder the walls together with a soldering iron from the inside. For this reason, some edges were coated with soldering tape and the walls of the sensor box were soldered together with a soldering iron from the outside. The final look of the constructed sensor is shown in Figure 6.10.

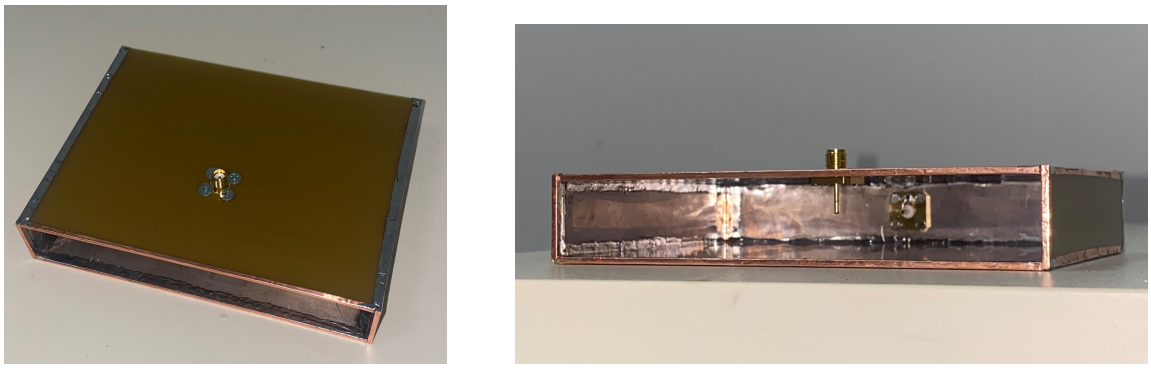

(a) View from the outside (b) View from the inside

Fig. 6.10: The constructed sensor

In Section 6.1, there was explained the process of simplification the production process, especially a model that represents the structure around the transformer tank gap. The structure will be substituted with a metal plate with a 6 mm high and 130 mm width slit. The metal plate can be seen in Figure 6.11.

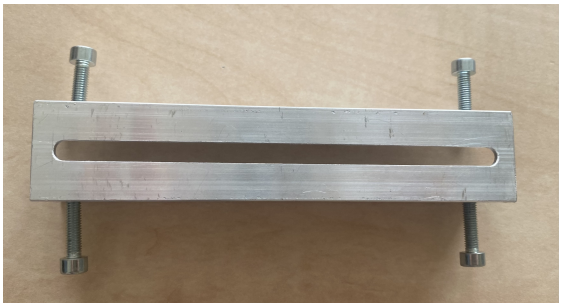

Fig. 6.11: The metal plate with 6 mm slit

The final design of the adapter with a mounted metal plate with a 6 mm slit from Figure 6.11 is shown in Figure 6.12.

Fig. 6.12: Final design of the sensor with the metal plate

7 Measurements

7.1 Preparation of testing area

All tests were performed in the shielded semi-anechoic chamber. A double ridged horn antenna from the manufacturer RF SPIN was used as a transmitting antenna. The type of antenna is DRH370 with a frequency range of 370MHz - 6 GHz and linear polarisation. As a receiving antenna to check the electric intensity of the field, a biconical antenna from manufacturer AARONIA is used. The parameters of the antenna are: type BICOLOG 20300 and a frequency range of 20MHz - 3GHz. The tests were measured and processed by the vector network analyzer Rohde&Schwarz ZVL6. with a frequency range of 9kHz to 6 GHz. The power output level was set to 20dBm, measuring the bandwidth 0.5 GHz - 3 GHz and the resolution bandwidth RBW = 10kHz. Calibration was performed before each measurement to prevent systematic error. In Figure 7.1, there is the graph of the relationship between the frequency of the signal and the antenna factor of a calibrated BICOLOG antenna. The most sensitive area of the antenna is for the signal with lower frequencies of the measured bandwidth.

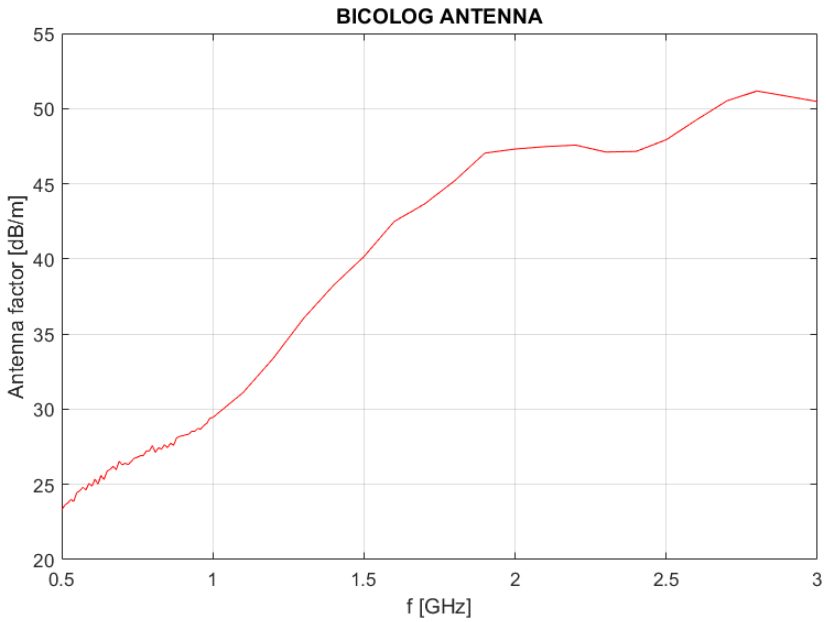

Fig. 7.1: The graph of the antenna factor of a calibrated BICOLOG antenna

The distance between the antennas and then the antenna and the sensor is 1 metre. This value was calculated to keep the receiving antenna and the sensor in the far-field distance. A far field is a region of electromagnetic field around the

transmitting antenna, in which transverse electric or magnetic fields with electric dipole characteristics are dominated. In this region, the absorption of the radiation does not feed back to the transmitting antenna. The apparatus, which measured the intensity of the actual EM field, is shown in Figure 7.2a and the measuring setup with constructed sensor is shown in Figure 7.2b.

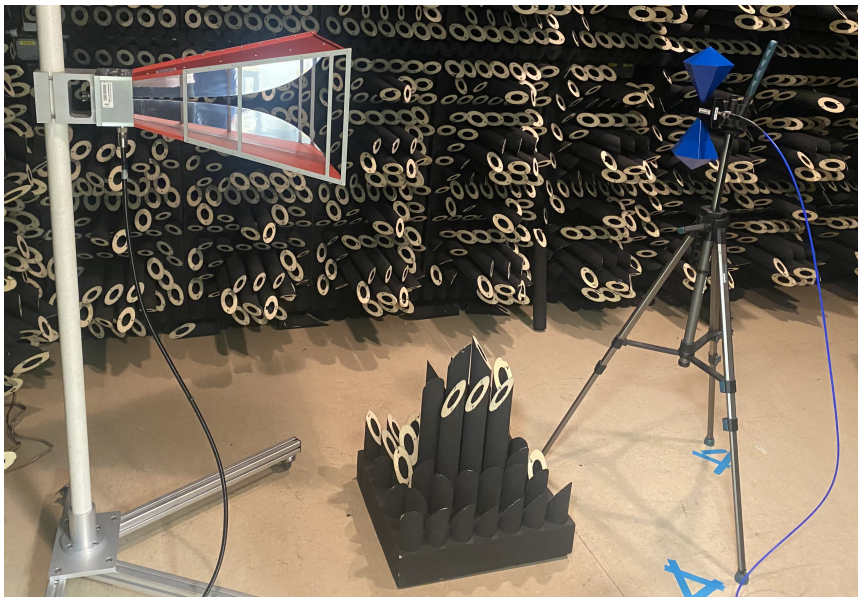

(a) Measuring the electric intensity of the present field

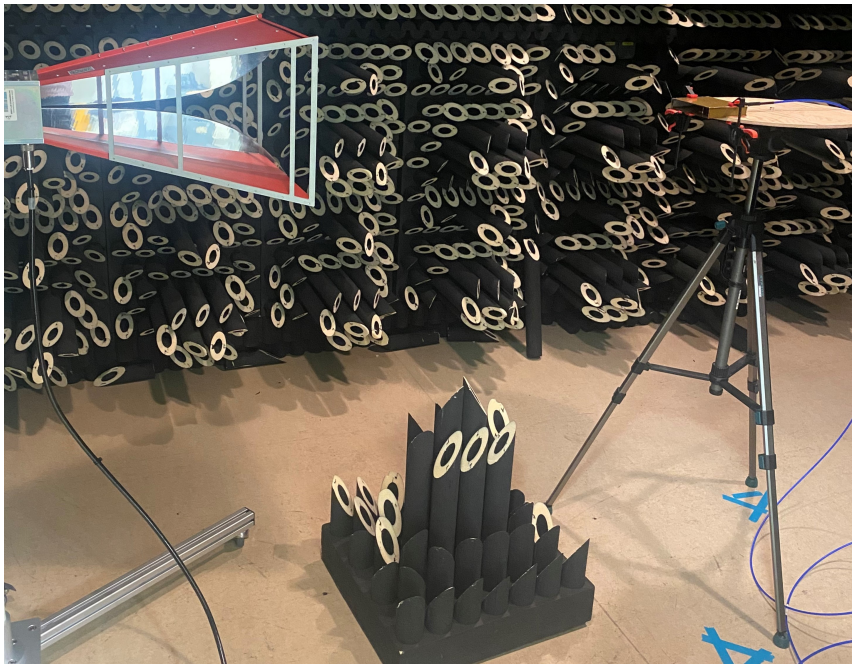

(b) Measuring the parameters of the sensor

Fig. 7.2: The measuring apparatus

All of the presented graphs are for vertical polarisation of the transmitting antenna. The tests were also performed for horizontal polarisation, but the sensor has a great attenuation according to our assumptions. The obtained values of S_{21} were from -70 to -100 dB. Therefore, this variant was not further studied.

7.2 S_{21} parameter

The parameter S_{21} describes the relationship between the input and output signal levels of a two-port. Within our measurement, it represents the power received at antenna 2 or the UHF sensor relative to the power input to antenna 1. The parameter is typically measured using a Vector Network Analyser (VNA). In the test, the mentioned VNA Analyser: Rohde&Schwarz ZVL6 with 20dBm output was used. The results of measurements were processed in the software MATLAB.

The results of the current probe tests are presented in Figure 7.3a and the loop probes test is shown in Figure 7.3b. The label "Adapter" in the graph legend of Figure 7.3 represents the 20mm height of the constructed sensor. The label "6 mm slot" means mounting a metal plate at the sensor entrance shown in Figure 6.11.

Characters of different options have almost the same tendency and behaviour as band-pass filters. The greatest attenuation occurs in the area of low and high frequencies. Nevertheless, the figure shows a considerable difference between the sizes of the probes. The longer probes have lower attenuation than the shorter probes.

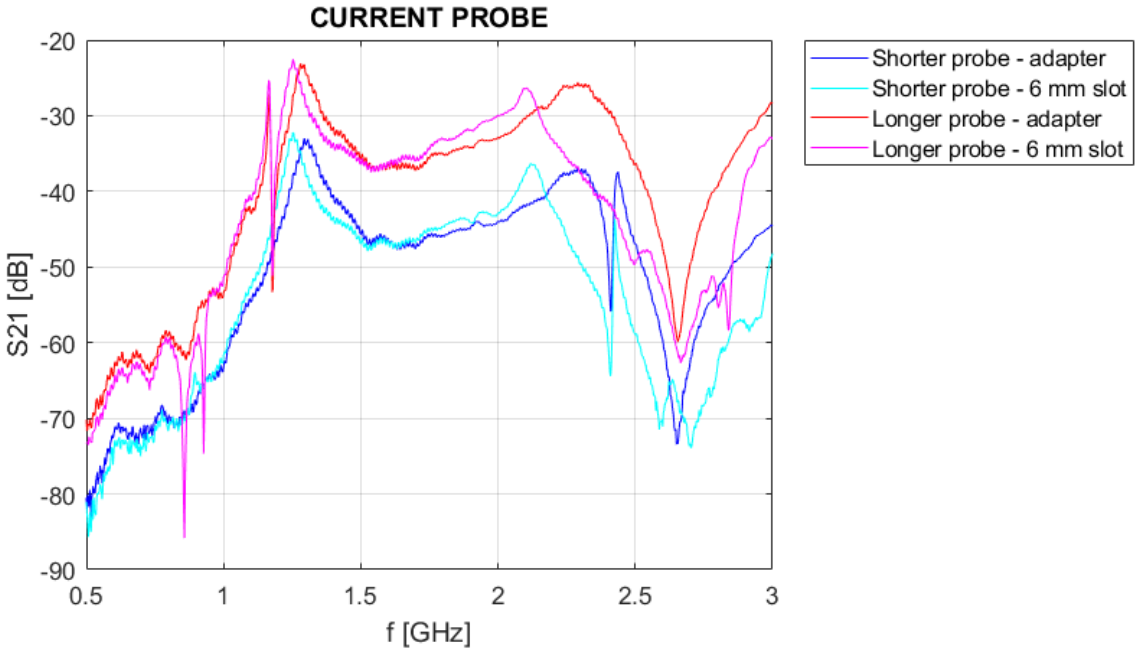

(a) Current probe

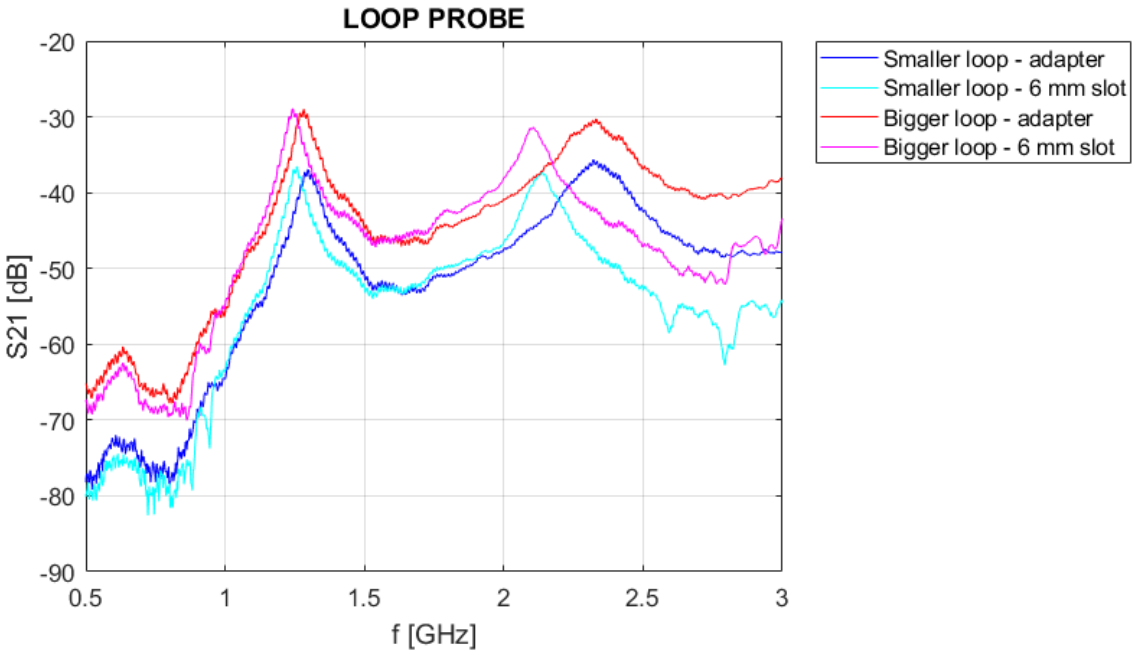

(b) Loop probe

Fig. 7.3: Measured S_{21} parameter

On the other hand, the longer monopole probe with a mounted 6mm slot has several drops. It is probably caused by the increased capacity between the probe and the opposite wall, leading to occurrence of resonance effect.

In conclusion, larger couplers extract more energy from the waveguide-like sensor and provide better sensor sensitivity. The best results were obtained with a longer monopole probe. But the bigger loop achieves a more stable trend without drops.

7.3 Antenna factor

Antenna factor is a parameter used for the electric field sensitivity characterization or an antenna. It defines the relationship between the electric field strength (E) around the antenna and the voltage on the output of the antenna by the antenna (U). For an electric field antenna, the resulting antenna factor AF is given by Equation 7.1.

$$AF = \frac{E}{U} \tag{7.1}$$

And in the logarithmic units, the above equation becomes

$$AF_{dB/m} = E_{dBV/m} - U_{dBV} \tag{7.2}$$

The relationship between the antenna factor and the frequency of the signal is shown in Figure 7.4a measured with current probes and in Figure 7.4b measured with loop probes.

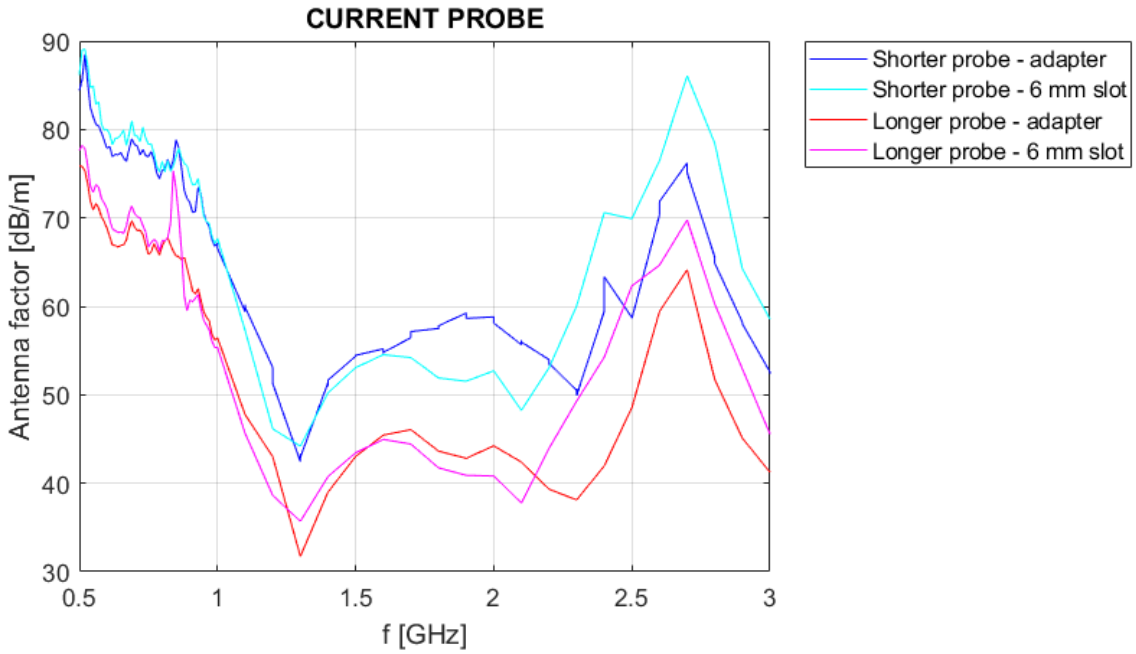

(a) Current probe

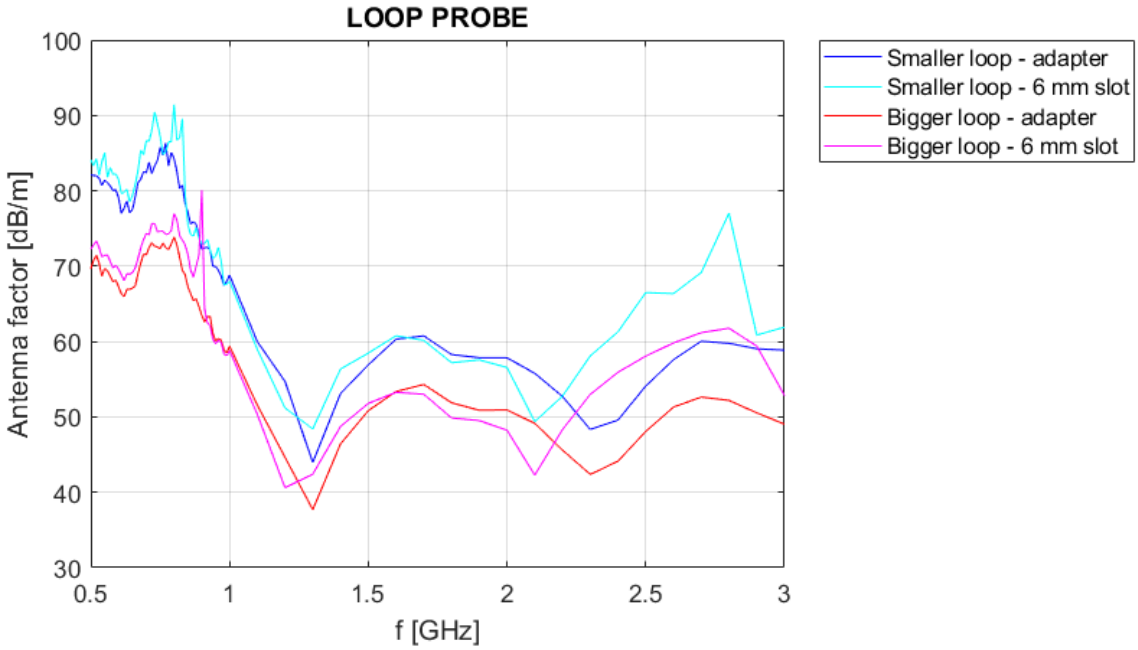

(b) Loop probe

Fig. 7.4: Measured Antenna factor for constructed sensor

The vector network analyser is able to measure and analyse only S_{21} parameter. Therefore, it is necessary to evaluate the parameters using additional equations. First, the BICOLOG antenna was used in order to measure the intensity of the electric field. By equation 7.3 the output power of the receiving BICOLOG antenna

was calculated. P_1 is the power set on the output of the RF SPIN antenna to transmit, for the test P_1 equals 20 dBm.

$$P_2 = S_{21_{db}} + P_1 \tag{7.3}$$

The output power values of the receiving BICOLOG antenna was used for the evaluation of voltage present on the output of the receiving antenna. Calculations were carried out with Equation 7.4. The resistance is 50 Ω.

$$U = \sqrt{50 \cdot P_2} \tag{7.4}$$

The BICOLOG antenna is a calibrated antenna with available values of its antenna factor, and using Equation 7.2 it was possible to calculate the intensity of the electric field at a distance of one metre from the transmitting antenna. Then the BICOLOG antenna was replaced by the constructed sensor. The apparatus is shown in Figure 7.2b. By Equation 7.3, the output power P_2, but this time for the designed adapter, was evaluated. The voltage in the sensor output was then calculated using equation 7.4. From the measured and calculated values of the intensity of the electric field, the voltage and by Equation 7.2, the values of antenna factor of constructed sensor were evaluated.

The antenna factor is a parameter that describes the possibility of the antenna to extract the actual intensity of the electric field and transform it into the voltage. Higher values of antenna factor mean that with the same intensity of an electric field, the sensor has a lower efficiency, the less energy is transformed. It can also be said that the sensor has a lower sensitivity. The graphs have similar behaviour; the sensor is the most sensitive in the frequency range from 0.4 to 2.4 GHz. In the area of low and high frequencies, the sensor is prone to a bad response.

7.4 Tilt and rotation of sensor

The sensor was also tested for different orientations with respect to the impinging electromagnetic wave: vertical tilt, 45- and 80-degree angles of slope, and horizontal rotation. The tests analysed the influence of the sensor location toward the source of the electromagnetic waves on the sensitivity of the adapter.

The antenna factors resulting from these tests are presented in Figure 7.5a for the current probe and Figure 7.5b for the loop probe. The monopole probe and loop coupling have similar behaviour; e.g. the horizontal rotation of the sensor has a bigger impact on the sensitivity than the tilt above the horizon. Overall, these results indicate that, for further analysis, it is more important to know the approximated horizontal location of the source of electromagnetic waves than the vertical location.

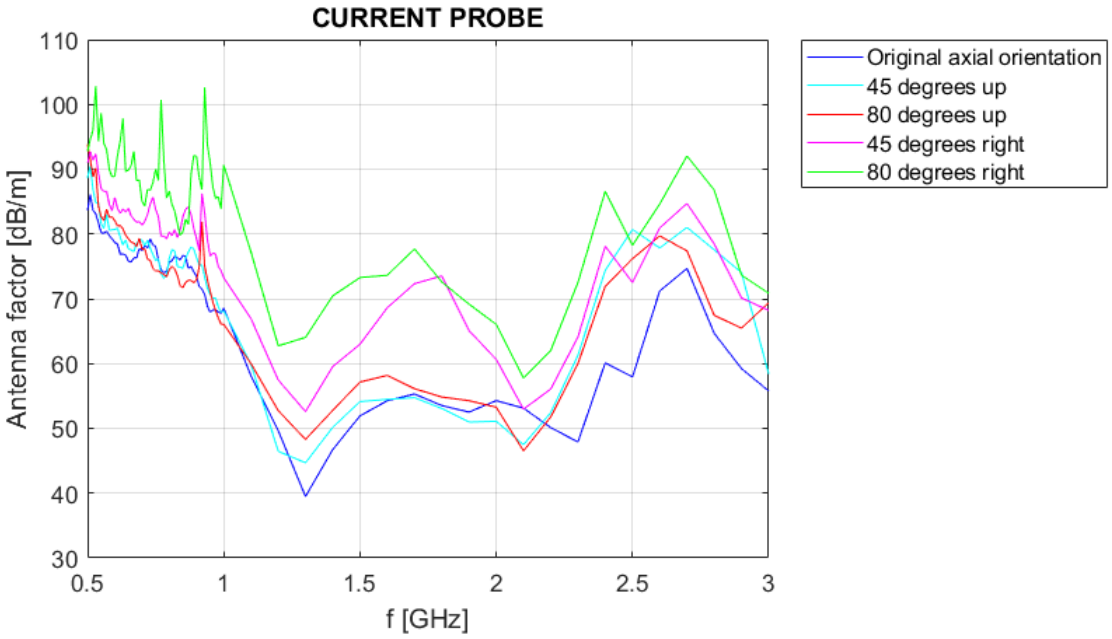

(a) Current probe

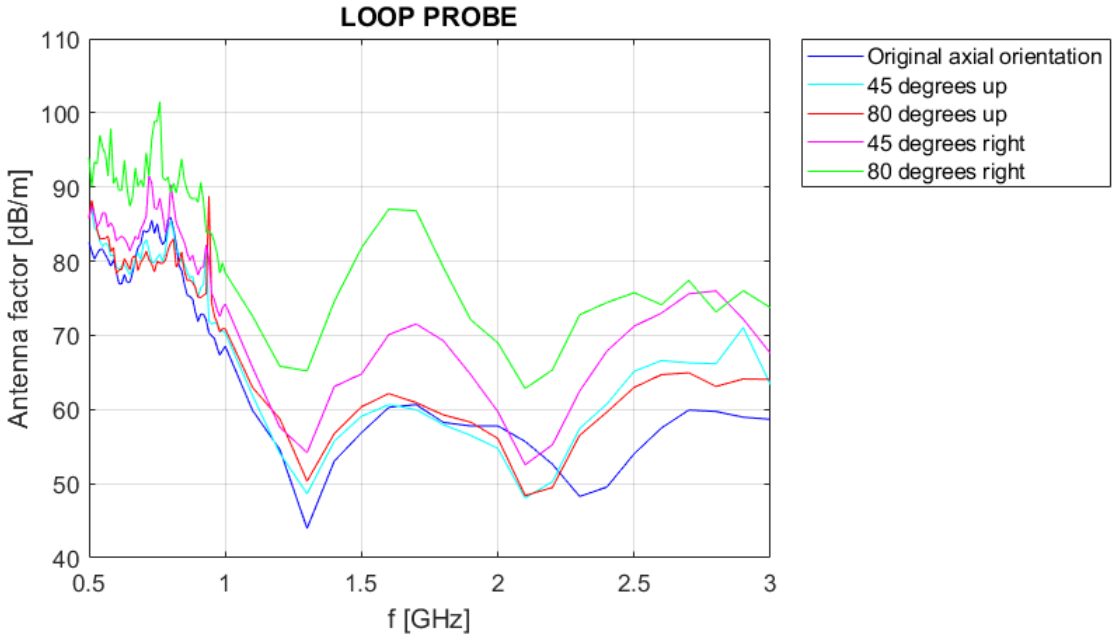

(b) Loop probe

Fig. 7.5: Various vertical and horizontal positions of sensor

7.5 Simulated data evaluation

For a better comparison of the simulation and measurements, it is important to unite the discussed parameters. For this reason, the value of the intensity of the electric and magnetic field was used for calculations of the antenna factor of the

simulated model. The model shown in Figure 5.1b was used for comparison. The values of the intensity of the magnetic and electric fields were determined from the graph in Figure 7.6a and Figure 7.6b.

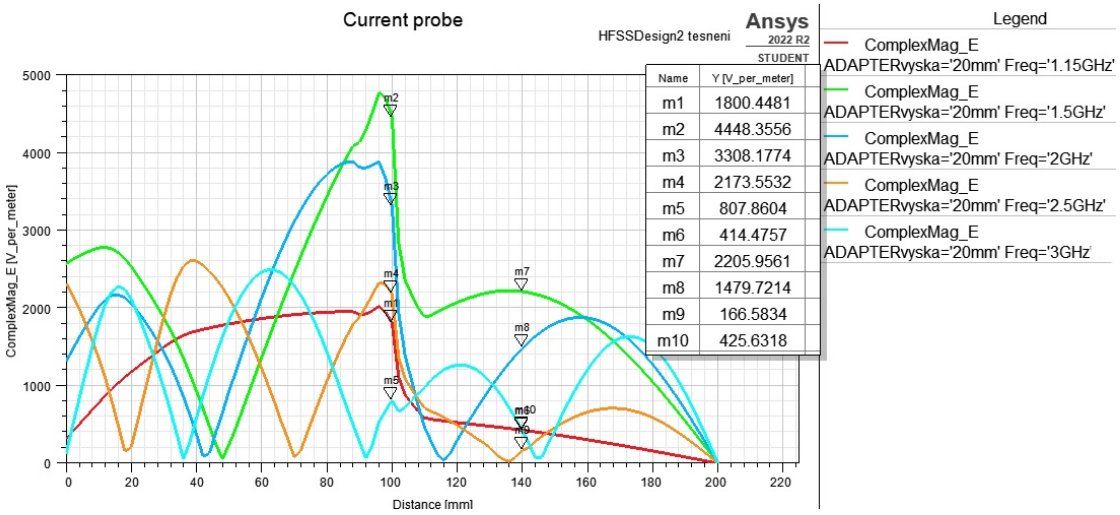

(a) Estimation of E intensity in simulation

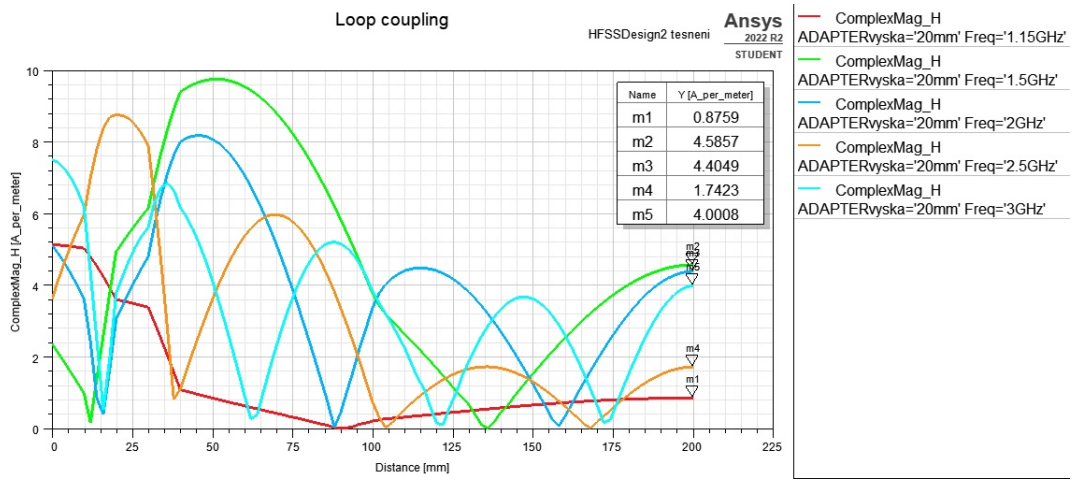

(b) Estimation of H intensity in simulation

Fig. 7.6: Graph used for the estimation of values of the intensity of E and H field in simulation

On the x-axis of the graphs, there is the parameter distance. This parameter represents the distance from the area where the electromagnetic waves enter the waveguide-like apparatus. In the 100mm distance, the entrance of the mentioned sensor is located. The current probe is approximately 140mm away from the entrance and the mounted loop coupler is 200mm away.

The electric intensity E_1, E_2 and magnetic intensity H were determined by the simulation results. The parameter E_1 represents the electric intensity at the entrance

of the sensor, E_2 presents the electric intensity in the area of the current probe, and H represents the magnetic intensity in the area of the loop. The voltage U at the output of the probe can be calculated using a line integral of the electric field intensity along the length of the monopole. Since we consider the field to be homogeneous in the vertical direction, the integral equation can be simplified to Equation 7.5, where d is the current probe length. The dimensions of the couplers are shown in Figure 6.5b.

$$U = E_2 \cdot d \tag{7.5}$$

Then with identified values of the intensity of the electric field E_1, the voltage U that would be measured and using Equation 7.1 was calculated the antenna factor for the chosen frequencies. Table 7.1 provides an overview of the simulated and evaluated data from the simulations. The parameter AF_{sim} represents the calculated antenna factor for simulations and AF_{meas} is the calculated antenna factor for measured values. Table 7.1 compares the antenna factor of the simulated and constructed adapter. It is normal that the simulation assumed a better sensitivity of the sensor. However, interestingly, the values of these parameters are not as diverse.

The evaluation of the values for the comparison of the simulated and constructed sensor with the loop probe was a little bit more difficult. Firstly, the value of the magnetic flux density was calculated using the following Equation:

$$B = \mu_0 \cdot H \tag{7.6}$$

where μ_0 is the permeability of the vacuum. Then, the approximate value of area S of the loop was calculated. The dimensions of the probes are shown in Figure 6.7b. The calculated values were used for the evaluation of the magnetic flux Φ using the Equation:

$$\Phi = B \cdot S \tag{7.7}$$

Equation 7.7 is simplified. The area of the loop is small, so it is assumed that there is a homogeneous field throughout the area of the loop. This means that B is a constant. Moreover, the vector of the area of the loop is parallel to the magnetic field vector, so the cosine of the angles between them equals one. The induced voltage around a closed loop is equal to the instantaneous rate of change of the magnetic flux through the loop. In equation form:

$$U = |\frac{-d\Phi}{dt}| \tag{7.8}$$

Then for the chosen frequency for which the antenna factor is evaluated, the harmonic balance is considered which means that the time derivative is transformed to the multiplication of $j \cdot \omega$. Then the module of the inducted voltage can be expressed with the following equation:

$$U = MOD(j \cdot \omega \cdot |\frac{-d\Phi}{dt}|) \tag{7.9}$$

From the voltage U values, the electric intensity E_1 of the entrance of the simulated sensor and the Equation 7.1 was calculated the antenna factor. The values of these calculations are presented in Table 7.1. The antenna factor values for the simulated and measured sensor differ slightly more. It is mainly caused by the mentioned simplification that was made during the calculations.

Monopole probe coupling					
h = 8.3 mm					
f [GHz]	E_1 [V/m]	E_2 [V/m]	U_{calc} [V]	AF_{sim} [dBm^{-1}]	AF_{meas} [dBm^{-1}]
0.15	1800	415	3.44	54.37	51.71
1.5	4448	2206	18.31	47.71	53.07
2	3308	1480	12.28	48.61	52.71
2.5	2174	167	1.39	63.88	69.91
3	808	426	3.54	47.17	58.54
h = 16.3 mm					
1.15	1800	415	6.76	48.51	42.14
1.5	4448	2206	36.96	41.85	43.44
2	3308	1480	24.12	42.74	40.82
2.5	2174	167	2.72	58.05	62.31
3	808	426	6.94	41.32	45.56
Loop coupling					
S = 2.55 x 4.9 mm					
f [GHz]	E_1 [V/m]	H [A/m]	U_{calc} [V]	AF_{sim} [dBm^{-1}]	AF_{meas} [dBm^{-1}]
1.15	1800	0.86	0.098	85.32	55.08
1.5	4448	4.59	0.679	76.32	58.47
2	3308	4.40	0.868	71.62	56.56
2.5	2174	1.74	0.429	74.09	58.07
3	808	4.00	1.571	56.68	61.91
S = 7.2 x 9.8 mm					
1.15	1800	0.86	0.551	70.28	45.48
1.5	4448	4.59	3.836	61.28	51.80
2	3308	4.40	4.903	56.58	48.24
2.5	2174	1.74	2.424	59.06	58.07
3	808	4.00	6.685	41.65	52.85

Tab. 7.1: Table of simulated and measured antenna factor values for monopole probe and loop coupling

8 Discussion

During the processing of the design of the waveguide-like sensor, simulations of theoretical conception, and measurements of the constructed sensor, significant results occurred. Some of the results can be studied in further analysis and they are not the subjects of these Bachelor's thesis. These conclusions are as follows:

- It was proved the theoretical statement, that the EM wave spreading through waveguide with frequencies lower than the cut-off frequencies is greatly attenuated. It can be seen in Figure 7.3
- At the same time, Figure 7.3 confirms that the simplification of the production process in Section 6.1 does not affect the behaviour of the apparatus. The main trait of the waveguide, the cutoff frequency, remains the same. So it can be used the same calculations to specify its value as in Section 4.4.1
- As can be seen in Figure 7.3, the sensor has a significant increase in sensitivity to EM waves with frequencies a little higher than the cut-off frequency. The basic cause of this peak has not yet been clarified and requires further analysis
- A significant difference was found between the smaller and bigger probes. The sensors with bigger probes, whether current or loop, both types provide better sensitivity to the EM field. This argument confirms Figure 7.3 and Figure 7.4. On the other hand, the bigger current probe has some drops in the characteristics shown in Figure 7.3a. They are caused by the resonance. Fortunately, it is in the area of frequencies that are anyway already attenuated by the waveguide
- The sensor, especially the one with loop probe, has the particular bandwidth, in which the sensor achieve the stable behaviour from the point of view of signal sensitivity and S_{21} parameter
- The sensors with loop probe have the better characteristic of sensitivity for signals with higher frequencies. The sensors with current probe have the decline in this area
- The bigger loop probe does not limit the bandwidth of the sensor as might be expected because of bigger value of inductance. This effect can be investigated in future studies
- It was detected the narrower directional characteristics of the sensor in the plane parallel to the main wall. It means that in practise applications, the sensor will be less sensitive in order to detect the UHF signals spreading from the direction parallel to this plane

Conclusion

Partial discharge is a dangerous phenomenon that occurs in power transformations. It harms the insulating material and influences the cooling effect. Partial discharges are related to the emission of sound, light, heat, electromagnetic energy or chemical reactions.

In the beggining, there was introduced different methods of partial discharge detection. The acoustic method analyses the pressure waves produced by the vaporization of the insulating material. The chemical method detects changes in the chemical composition of the transformer oil. The emitted light is tested by an optical method. Then, there is the electrical method: IEC 60270 and high frequency current transformer (HFCT) sensors. Both are attracted to the electrical effects of partial discharge. The last group presented, connected with electromagnetic induction, was electromagnetic detection, TEV and UHF method. The last mentioned will be used for the design of our sensor.

UHF method uses different types of sensors, in other words antennas. Moreover, these sensors have two versions: internal and external. For the design, the external type is used , because the sensor will be situated in the gap of the transformer tank. The gap has traits similar to those of a rectangular waveguide. Therefore, with available dimensions of the gap, the cutoff frequency was calculated. The designed waveguide has a cut-frequency f_c equal to **1.15 GHz**.

To distribute or remove the energy from the waveguide, it is used waveguide couplers. There are three types, but for the design only two of them are used: current and loop probes. In the case of the current probes, a coaxial cable probe is formed in the monopole probe and inserted into the waveguide adapter. This probe should be in the middle of the longer dimension a of the waveguide and 53 mm away from the shorted end. In the case of loop coupling, the end of the coaxial cable has a loop shape and is placed on the sensors' boundaries.

For better design of the sensor were performed the simulations of the waveguide-like apparatus in the software Ansys HFSS. Simulations verified the behaviour of the electromagnetic field inside the sensor. As a consequence of the simulation results, the height of the adapter was specified to be **20 mm**. Furthermore, it was confirmed that the monopole probe should be **approximately 60 mm from the back side**. The loop should be placed in the middle of the back side of the sensor.

Then the simulated sensor was constructed. It is made of a FR4 substrate. The plates were overlaid with a layer of silver to increase electrical conductivity and protect the copper layer against oxidation. The connectors are attached to the sensor box with screws. This construction provides the possibility of a single sensor box with changeable probes. The tests were performed for smaller and larger sizes

of waveguide couplers to test the sensitivity of the sensor.

The tests of the constructed sensor were performed in the shielded semi-anechoic chamber. The transmitting and receiving antennas were calibrated antennas. The receiving antenna evaluates the intensity of the electric intensity. The measurements were analysed with a vector network analyser. The first measurement focused on the **S**21 **parameter**. The results confirmed the theoretical hypothesis that **the larger monopole probe and loop have a smaller attenuation**. The second measurement was orientated to the evaluation of the **antenna factor**. The sensor is **less sensitive to lower and higher frequencies**. Moreover, **the smaller current and loop probe are less sensitive** to electromagnetic field. In the third measurement, the sensor was tested for different vertical orientation: original axial orientation, the 45 and 80 degrees angle of slope and rotation. **The rotation of the sensor has a bigger impact on the sensitivity than the tilt above the horizon.**

In the end, there is the comparison of the antenna factor calculated for simulations and measurements. The values of the antenna factor are slightly different for the current probe. The antenna factor values for the loop probes differ more. It is mainly caused by the simplification that was made during the calculations of the antenna factor of the simulated model. Taken together, **the results show that the design and construction of the adapter can be considered successful**. These tests provide the basis for the possibility of applying the designed and constructed external sensor to test the occurrence of partial discharge inside the transformer tank. The results are promising and should be tested for the real transformer in the power plant Temelín.

Bibliography

[1] ČEZ. NPP Dukovany [online]. [Cit. 2022-11-26]. Available at: https://www.cez.cz/en/energy-generation/nuclear-power-plants/dukovany.

[2] ČEZ. NPP Temelin [online]. [Cit. 2022-11-26]. Available at: https://www.cez.cz/en/energy-generation/nuclear-power-plants/temelin.

[3] Jaspreet Singh, Sanjeev Singh, 2016, Transformer Failure Analysis:Reasons and Methods, INTERNATIONAL JOURNAL OF ENGINEERING RESEARCH TECHNOLOGY (IJERT) ACMEE – 2016 (Volume 4 – Issue 15). ISSN 2278-0181 [online]. [Cit. 2022-11-26]. Available at: https://www.ijert.org/transformer-failure-analysisreasons-and-methods.

[4] ELECTRICAL-TECHNOLOGY. Different Parts of transformer and their functions [online]. [Cit. 2022-11-26]. Available at: https://www.electrical-technology.com/2021/09/parts-of-transformer.html.

[5] VUT v Brně: International Electrotechnical Commission, IEC 60076-3: Power transformers - Part 3: Insulation levels, dielectric tests and external clearances, Geneva, Switzerland: IEC, 2015.

[6] Mithun Mondal G.B. Kumbhar (2018) Detection, Measurement, and Classification of Partial Discharge in a Power Transformer: Methods, Trends, and Future Research, IETE Technical Review, 35:5, 483-493. [online]. [Cit. 2022-11-27] https://doi.org/10.1080/02564602.2017.1335244.

[7] Yaacob, M.M., Alsaedi, M.A., Rashed, J.R. et al. Review on partial discharge detection techniques related to high voltage power equipment using different sensors. Photonic Sens 4, 325–337 (2014). [online]. [Cit. 2022-11-27] https://doi.org/10.1007/s13320-014-0146-7.

[8] Jiangdong Deng, Hai Xiao, Wei Huo, Ming Luo, Russ May, Anbo Wang, Yilu Liu, Optical fiber sensor-based detection of partial discharges in power transformers, Optics Laser Technology, (Volume 33, Issue 5), 2001,ISSN 0030-3992. [online]. [Cit. 2022-11-27] Available at: https://doi.org/10.1016/S0030-3992(01)00022-6.

[9] A. Itose, M. Kozako and M. Hikita, "Partial discharge detection and induced surface current analysis using transient earth voltage method for high voltage

equipment," 2016 International Conference on Condition Monitoring and Diagnosis (CMD), 2016, pp. 456-460 [online]. [Cit. 2022-11-28] Available at: https://doi.org/10.1109/CMD.2016.7757859.

[10] Luo, G. (2013). Transient earth voltage (TEV) based partial discharge detection and analysis. Doctoral thesis, Nanyang Technological University, Singapore [online]. [Cit. 2022-11-28] Available at: https://doi.org/10.32657/10356/54865.

[11] Álvarez, F.; Garnacho, F.; Ortego, J.; Sánchez-Urán, M.Á. Application of HFCT and UHF Sensors in On-Line Partial Discharge Measurements for Insulation Diagnosis of High Voltage Equipment. Sensors 2015, 15, 7360-7387. [online]. [Cit. 2022-11-28] Available at: https://doi.org/10.3390/s150407360.

[12] Álvarez, F.; Garnacho, F.; Ortego, J.; Sánchez-Urán, M.Á. Application of HFCT and UHF Sensors in On-Line Partial Discharge Measurements for Insulation Diagnosis of High Voltage Equipment. Sensors 2015, 15, 7360-7387. [online]. [Cit. 2022-11-28] Available at: https://doi.org/10.3390/s150407360.

[13] X. Hu, W. H. Siew, M. D. Judd and X. Peng, "Transfer function characterization for HFCTs used in partial discharge detection," in IEEE Transactions on Dielectrics and Electrical Insulation, vol. 24, no. 2, pp. 1088-1096, April 2017. [online]. [Cit. 2022-11-28] Available at: https://doi.org/10.1109/TDEI.2017.006115.

[14] Tenbohlen, Stefan & Coenen, S. & Siegel, Martin & Linn Thomas & Markalous, Sacha & Mraz, Petr & Beltle, Michael & Naderian, A. & Schmidt, Volker & Fuhr, Jitka & Fehlmann, P. & Cselko, Richard & Gatechompol, R. & Hässig, Markus & Hoek, Stefan & Judd, Martin & Kempf, Ulrich & Schwarz, R. & Söller, Markus & Weber, Marc. (2022). Improvements to PD measurements for factory and site acceptance tests of power transformers, Cigre Technical Brochure 861. [Cit. 2022-11-28] ISBN: 978-2-85873-566-2 .

[15] DREXLER, Petr, et al. A Sensor System for Detecting and Localizing Partial Discharges in Power Transformers with Improved Immunity to Interferences. Sensors. 2019, 19(4) [online]. [Cit. 2022-12-04] Available at: https://doi.org/10.3390/s19040923.

[16] D. Liu, A. Guan, S. Zheng, Y. Zhao, Z. Zheng and A. Zhong, "Design of External UHF Sensor for Partial Discharge of Power Transformer," 2021 IEEE 2nd China

International Youth Conference on Electrical Engineering (CIYCEE), 2021, pp. 1-5. [online]. [Cit. 2022-12-04] Available at: https://doi.org/10.1109/CIYCEE53554.2021.9676823.

[17] Čáp, Martin. Detekce a prostorová lokalizace částečných výbojů ve výkonových transformátorech metodou UHF [online]. Brno, 2023 [cit. 2022-12-05]. Dizertační práce. Vysoké učení technické v Brně, Fakulta elektrotechniky a komunikačních technologií, Ústav radioelektroniky. Školitel práce doc. Ing. Petr Drexler, Ph.D. Available at: https://www.vut.cz/studenti/zav-prace/detail/96993.

[18] J. Lopez-Roldan, T. Tang and M. Gaskin, "Optimisation of a sensor for onsite detection of partial discharges in power transformers by the UHF method," in IEEE Transactions on Dielectrics and Electrical Insulation, vol. 15, no. 6, pp. 1634-1639, December 2008. [online]. [Cit. 2022-12-12] Available at: https://doi.org/10.1109/TDEI.2008.4712667.

[19] Zhang, X.; Zhang, G.; Li, Y.; Zhang, J.; Huang, R. On the Feasibility of Gap Detection of Power Transformer Partial Discharge UHF Signals: Gap Propagation Characteristics of Electromagnetic Waves. Energies 2017, 10, 1531 [online]. [Cit. 2022-12-12] Available at: https://doi.org/10.3390/en10101531

[20] Electronics Notes. Waveguide Cutoff Frequency [online]. [Cit. 2022-12-13]. Available at: https://www.electronics-notes.com/articles/antennas-propagation/rf-feeders-transmission-lines/waveguide-cutoff-frequency.php.

[21] Krishnan, Remya Nair, K R M. (2018). Fastener Spacing Tightening Torque of Gasket Joints of Oil Filled Transformers. Indian Journal of Science and Technology. 11. 1-4. [online]. [Cit. 2022-12-15] Available at: https://doi.org/10.17485/ijst/2018/v11i11/119545.

[22] Matsuno R, Takagaki Y, Ito T, Yoshikawa H, Takamatsu S, Takahara A. Relationship between the Relative Dielectric Constant and the Monomer Sequence of Acrylonitrile in Rubber. ACS Omega [online]. [Cit. 2022-12-27] Available at: https://doi.org/10.1021/acsomega.0c02084.

[23] Integrated publishing, Inc., ELECTRONICS TECHNICIAN, VOLUME 07– ANTENNAS AND WAVE PROPAGATION, [online]. [Cit. 2022-12-25] Available at: https://electronicstechnician.tpub.com/14092/.